SCIENTIFIC REPORTS

OPEN

SUBJECT AREAS:
METAL-ORGANIC FRAMEWORKS
MATERIALS FOR DEVICES
STRUCTURAL MATERIALS
PHOTONIC DEVICES

Received
6 December 2013

Accepted
22 April 2014

Published
12 May 2014

Correspondence and requests for materials should be addressed to K.K. (kamata.k.ab@m.titech.ac.jp); T.I. (iyoda.t.aa@m.titech.ac.jp) or M.H. (hangyo@ile.osaka-u.ac.jp)

Spirulina-Templated Metal Microcoils with Controlled Helical Structures for THz Electromagnetic Responses

Kaori Kamata[1,2], Zhenzi Piao[1], Soichiro Suzuki[3], Takahiro Fujimori[3], Wataru Tajiri[3], Keiji Nagai[1,3], Tomokazu Iyoda[1,2,3], Atsushi Yamada[2,4], Toshiaki Hayakawa[2,5], Mitsuteru Ishiwara[6], Satoshi Horaguchi[6], Amha Belay[7], Takuo Tanaka[2,8], Keisuke Takano[9] & Masanori Hangyo[9]

[1]Iyoda Supra-Integrated Material Project, Exploratory Research for Advanced Technology (ERATO), Japan Science and Technology Agency (JST), 4259 Nagatsuta-Cho, Midori-Ku, Yokohama, Kanagawa 226-8503, Japan, [2]Research Society for Biotemplate Technology, 4259 Nagatsuta-Cho, Midori-Ku, Yokohama, Kanagawa 226-8503, Japan, [3]Division of Integrated Molecular Engineering, Chemical Resources Laboratory, Tokyo Institute of Technology, 4259 Nagatsuta-Cho, Midori-Ku, Yokohama, Kanagawa 226-8503, Japan, [4]Technology and Engineering Department, Materials Division, Sumitomo Metal Mining Co. Ltd., 5-11-3 Shimbashi, Minato-Ku, Tokyo 105-8716, Japan, [5]Advantest Laboratories Ltd., 48-2 Matsubara, Kami-Ayashi, Aoba-Ku, Sendai, Miyagi 989-3124, Japan, [6]DIC LIFETEC Co., Ltd., 12 Yawata-Kaigandori, Ichihara, Chiba 290-8585, Japan, [7]Earthrise Nutritionals, LLC., 113 E. Hoober Road Calipatria, CA 92233, USA, [8]Metamaterials Laboratory, Advanced Science Institute, RIKEN, Wako, Saitama 351-0198, Japan, [9]Institute of Laser Engineering, Osaka University, 2-6 Yamadaoka, Suita, Osaka 565-0871, Japan.

Microstructures in nature are ultrafine and ordered in biological roles, which have attracted material scientists. *Spirulina* forms three-dimensional helical microstructure, one of remarkable features in nature beyond our current processing technology such as lithography in terms of mass-productivity and structural multiplicity. *Spirulina* varies its diameter, helical pitch, and/or length against growing environment. This unique helix is suggestive of a tiny electromagnetic coil, if composed of electro-conductive metal, which brought us main concept of this work. Here, we describe the biotemplating process onto *Spirulina* surface to fabricate metal microcoils. Structural parameters of the microcoil can be controlled by the cultivation conditions of *Spirulina* template and also purely one-handed microcoil can be fabricated. A microcoil dispersion sheet exhibited optically active response attributed to structural resonance in terahertz-wave region.

People have been fascinated by highly complex microstructures produced in nature[1]. Natural materials are sophisticatedly organized in response to specific functions, whose systematical organizing processes are superior to any engineering routes for smart materials in the light of multiplicity, optimal integration, and low energy consumption. In naturally occurring microstructures, important feature is their high dimensionality, which stimulates material scientists to design functional materials. Biomimetics or bioinspiration[2–4], learning microstructures produced in nature, have drawn attention as one of breakthroughs on material science and processing. But profound understanding of formation mechanism established under natural selection process must be required to develop the biomimetic process. In fact, we have suggested collaborating with nature, *i.e.*, biotemplating process, which directly borrows the natural microstructures for new material fabrications (Fig. 1). A concept of this process can lead to mass productivity with less energy. Main issue is how to control the natural microstructures. If we can find effective factors controlling the structures from various environmental conditions, the biotemplating process would have unlimited potential and will be global strategy for material development. We have focused three-dimensional helical feature in nature as biotemplate candidate[5]. Helical microalgae, *Spirulina* (*Arthrospira platensis*)[6,7] naturally shaping left-handed (LH) open helical structure and already commercialized as nutritional supplements or food materials[8], was employed in this study. Its helical structure is very sensitive against the environmental conditions, which should be strong advantage to exploit a variety of diameter, pitch, and handedness. Development of biotemplating process using *Spirulina* can achieve mass production of microcoil (μcoil), which is currently manufactured by precision machining or lithography one by one. Since Chen et al. first coated the *Spirulina* surface with magnetic ferrite[9], several biotemplating processes using the *Spirulina*

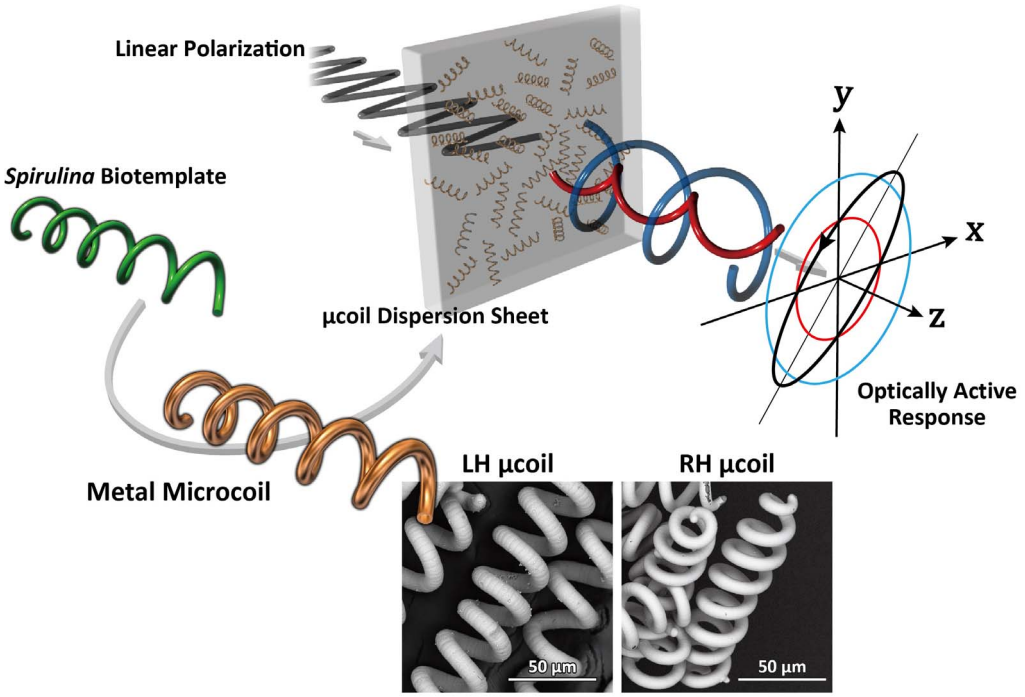

Figure 1 | Fabrication of *Spirulina*-templated microcoil (μcoil) and its optical activity against THz wave. The *Spirulina* (*Arthrospira platensis*) was utilized as biotemplate to mass fabricate 3D helical μcoils. An enantiomeric pair of left-handed (LH) and right-handed (RH) μcoils can be fabricated with 100% of optical purities as SEM images show. The THz time-domain spectroscopies with polarimetric analyses (THz-TDS-PA) of paraffin sheets containing the μcoils were measured to examine optical activities and structural resonances based on the helical structures.

have been reported in the field of material science. However, no function specific to its helical microstructure has yet been discovered.

Results

Structure-controllability of *Spirulina* biotemplate. The LH helix of *Spirulina* is a common structure found in nature and easily obtained as the stock strain from culture collections. Under the conventional cultivation condition[10], average feature size of the LH *Spirulina* (Fig. 2a) were 6 μm in wire diameter (d), 43 μm in coil diameter (D), 174 μm in free length of coil (L_{free}), 74 μm in coil pitch (L_{free}/N), 2.4 in turn number (N), and 29 ° in pitch angle (α) (for graphical illustration of the symbols, see Fig. S1). The number of *Spirulina* in 1 mL increased from 10^2 to 10^5 within one week (Methods and Fig. S2). During the cultivation, the d, D, and L_{free}/N remained with narrow size distributions (around 5–15% of relative standard deviation, RSD), while the L_{free} had a higher RSD around 20% because *Spirulina* grows along the long axis direction (Fig. S3). It has been known that the *Spirulina* forms various helical features and even linear shape under different environments. In this study, the L_{free}/N was systematically controlled by varying cultivation temperature and light intensity (Methods and SI-II)[11]. The series of LH *Spirulina* with five different helical features in Fig. 2 are numbered as LH template-1 to -5. Linear *Spirulina* often found in laboratory cultivation of regular helical strains was obtained in pure culture (Fig. 2f). Such flexible morphologies against the environment can achieve distinction as microstructured-materials separately from commonly-used genetic control.

***Spirulina*-based biotemplating process.** We have designed the biotemplating process using electroless plating technique, which can generate smooth metal layer selectively on surface of targeting object to be plated. In this study, the process includes (i) fixation of *Spirulina*, (ii) Pd catalyzation (Pd nanoparticle adsorption as plating catalyst nuclei[12,13]), and (iii) copper electroless plating (Methods, see also Supplementary SI-III). The process (i) employed general method of tissue fixation by glutaraldehyde, which cross-links amine groups of amino-acid side chains in proteins[14]. The process (ii) includes two steps with Pd ion adsorption and reduction of the Pd ion to form the metallic Pd, which can work as catalyst oxidizing reducing reagent for the metal deposition from the plating bath. For the electroless plating, bath load, *i.e.*, the total surface area of *Spirulina* to amount of plating bath, was adjusted to be 200 cm^2/L. In the laboratory scale with 1 L of plating bath, one batch from 20 mL of the *Spirulina* cultivation medium with 10^5 mL^{-1} in *Spirulina* concentration gave approximately 2 million μcoils (90 mg, 80% yield). The resulting μcoils were quantitatively and qualitatively characterized by ICP, XPS, XRD, and EDX-SEM at different stage of biotemplating process (for the detailed information, see supplementary SI-III). It was found that the Pd catalyst was adsorbed to the surface as well as inside the tissue of *Spirulina* with almost 2 vol% in volume fraction to the *Spirulina*. The μcoil contained the metallic Pd of >80% and a little amount of PdO_x in the nanoparticles.

The copper layer deposited on the *Spirulina* was consisting of the metal (>90% in content) with the oxides at the surface. The μcoils looked reddish brown with metallic luster and had tubular structure with around 550 nm in thickness, whose interior space still included the fixed *Spirulina* template (Fig. S15). The thickness can be controlled by changing the plating time and also the bath load, here, we demonstrated with 200 cm^2/L in the bath load (20-mL loading amount) to obtain the thickness enough to exhibit bulk-like electric property. The efficiency of Cu deposition and relationship between the bath load and the thickness were discussed in supplementary SI-IV. The optical micrographs of μcoils (LH μcoil-1 to -5) fabricated from corresponding LH template-1 to -5 are shown in Figure 2g-2k along with straight copper wire (Fig. 2l) from the linear strain. Emphasis should be placed on that the microstructures after the biotemplating processes were faithfully transferred from those of the *Spirulina* templates, for example, in case of LH μcoil-1, d = 7.0 μm (15%RSD), D = 41 μm (14%), L_{free} = 174 μm (26%), L_{free}/N = 77 μm (9%), N = 2.3, and α = 31 ° (see also Fig. S16).

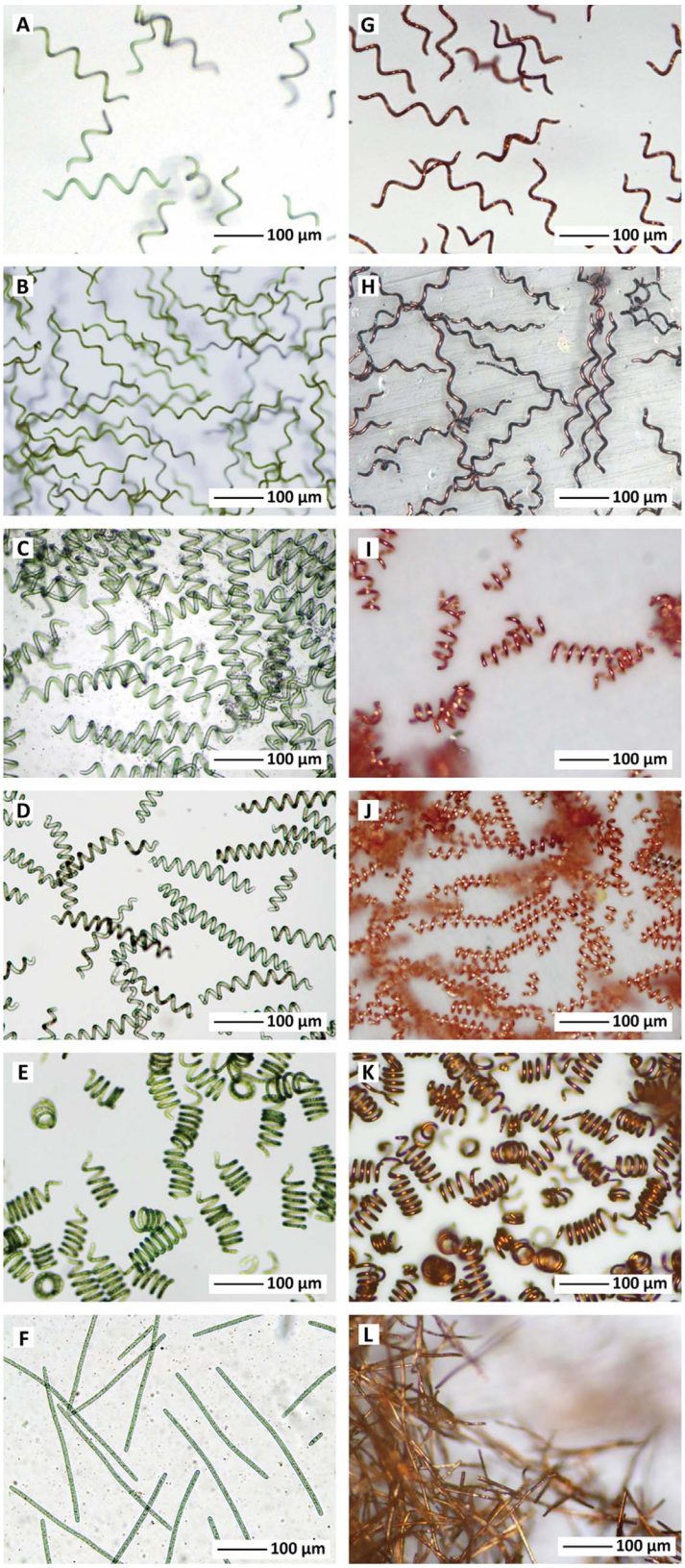

Figure 2 | Left-handed (LH) *Spirulina*-templated microstructures. The *Spirulina* basically forms LH helix but its structural parameters such as helical pitch, length, number of turns, and handedness are of variety based on a kind of strains. Sensitive strain, NIES-46, gradually tightens the helical pitch as the cultivation proceeded with stronger light intensity and higher temperature. The systematic adjustment of the helical pitch, L_{free}/N, can be demonstrated; (a)-(e), LH template-1 to -5. (f) Linear strain was prepared by the pure cultivation of laboratory-derived single trichome. The biotemplating process was successfully carried out to generate the copper μcoils whose structures are followed by those of LH templates: (coil number, L_{free}/N); (g) LH μcoil-1, 77 μm; (h) LH μcoil-2, 55 μm; (i) LH μcoil-3, 27 μm; (j) LH μcoil-4, 20 μm; (k) LH μcoil-5, 16 μm. (l) The straight copper wire was also properly templated from the linear strain.

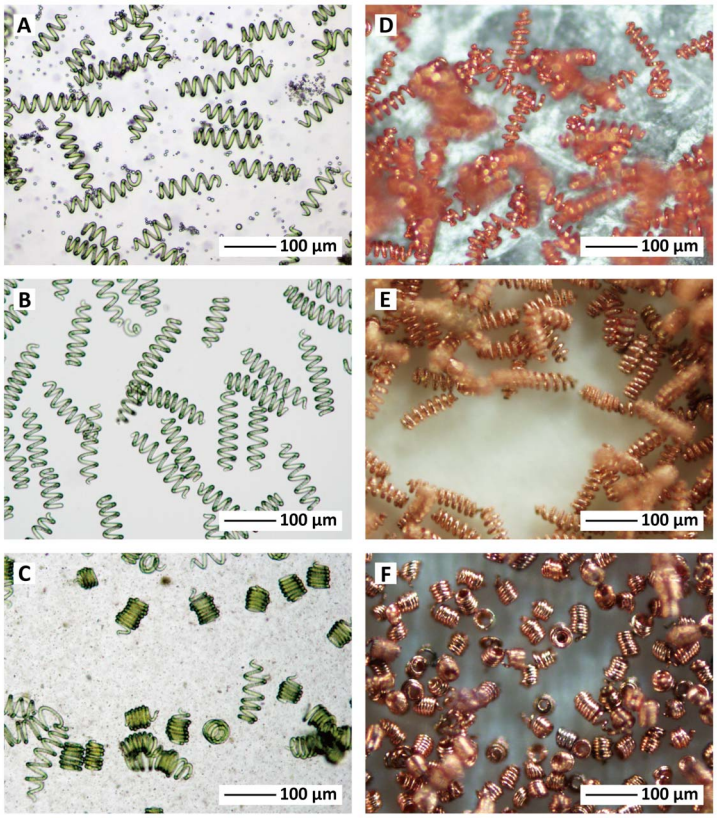

Figure 3 | Right-handed (RH) *Spirulina* and their biotemplated products. RH template-1 to -3 with three different L_{free}/Ns, (a) – (c), generated the corresponding RH μcoils: (coil number, L_{free}/N); (d) RH μcoil-1, 19 μm; (e) RH μcoil-2, 14 μm; (f) RH μcoil-3, 6 μm.

Right-handed (RH) strains of *Spirulina* are rare but they are found both in nature and in culture. Reversal of helical handedness from left to right and vice versa has been observed and ascribed to genetic drift or environmental factors like temperature uplift or mechanical stress[15]. One such RH strain obtained from Earthrise Nutritionals, California, USA, was grown in pure culture from a single trichome. The RH *Spirulina* was more tightly coiled smaller than around 20 μm in L_{free}/N. The RH templates and the corresponding μcoils were prepared in the same manner as the LH series (Fig. 3 and Fig. S17). The structural parameters for all of μcoils and referenced samples are summarized in Table 1.

Can the μcoil behave as chiral electromagnetic material? We prepared dispersion silicon sheets of LH μcoil-1 for transmission and reflection spectroscopies in the region of millimeter wave with free space method (Fig. 4a and 4b, SI-VI). The logarithmic transmittance decreased as the concentration of μcoil was increased. Reflection components were almost constant against the

Table 1 | The geometric parameters of μcoil

Parameters	wire diameter	coil diameter	free length of pitch	number of turn	free length of coil	length of wire for one pitch	length of wire for one coil	pitch angle[1]	theoretical frequency region[2]	detected frequency region[3]
symbol	d	D	L_{free}/N	N	L_{free}	L_{wire}/N	L_{wire}	α	F_d	F_0
Units	μm	μm	μm	-	μm	μm	μm	degree	THz	THz
LH μcoil-1	7	41	77	2.3	174	150	339	30.9	0.67–1.33	0.5–1.5
LH μcoil-2	7	26	56	4.5	248	99	441	34.0	1.02–2.03	0.5–1.6
LH μcoil-3	9	35	27	5.7	153	113	642	13.8	0.88–1.77	0.5–1.9
LH μcoil-4	7	22	20	5.6	111	72	399	16.1	1.39–2.78	0.5–2.1
LH μcoil-5	8	46	16	5.1	81	145	736	6.3	0.69–1.38	0.4–1.2
RH μcoil-1	8	30	19	6.8	130	96	658	11.4	1.04–2.08	0.4–1.6
RH μcoil-2	8	30	14	7.9	110	95	749	8.5	1.05–2.10	0.3–2.0
RH μcoil-3	6	33	6	7.0	44	104	725	3.5	0.96–1.93	*n/a*
Straight wire	6	*n/a*	*n/a*	*n/a*	320	*n/a*	320	90	*n/a*	*n/a*
Freeze-dried *Spirulina*	5	20	44	4.3	188	77	328	35	1.30–2.61	*n/a*

[1]The pitch angle equals to $\tan^{-1}(L_{free}/N)/(\pi D)$.
[2]The frequency region means that the μcoil emits elliptical polarization with the opposite handedness within the range and can be predicted with $L_{wire}/N < \lambda_0 < 2L_{wire}/N$, as defined in helical antenna array. The wave propagates in paraffin matrix ($n = 1.5$), so that the frequency is given by $F_d = \frac{300 \times n}{\lambda_0}$.
[3]The frequency region was defined as the difference between two peaks of ellipticity angles.

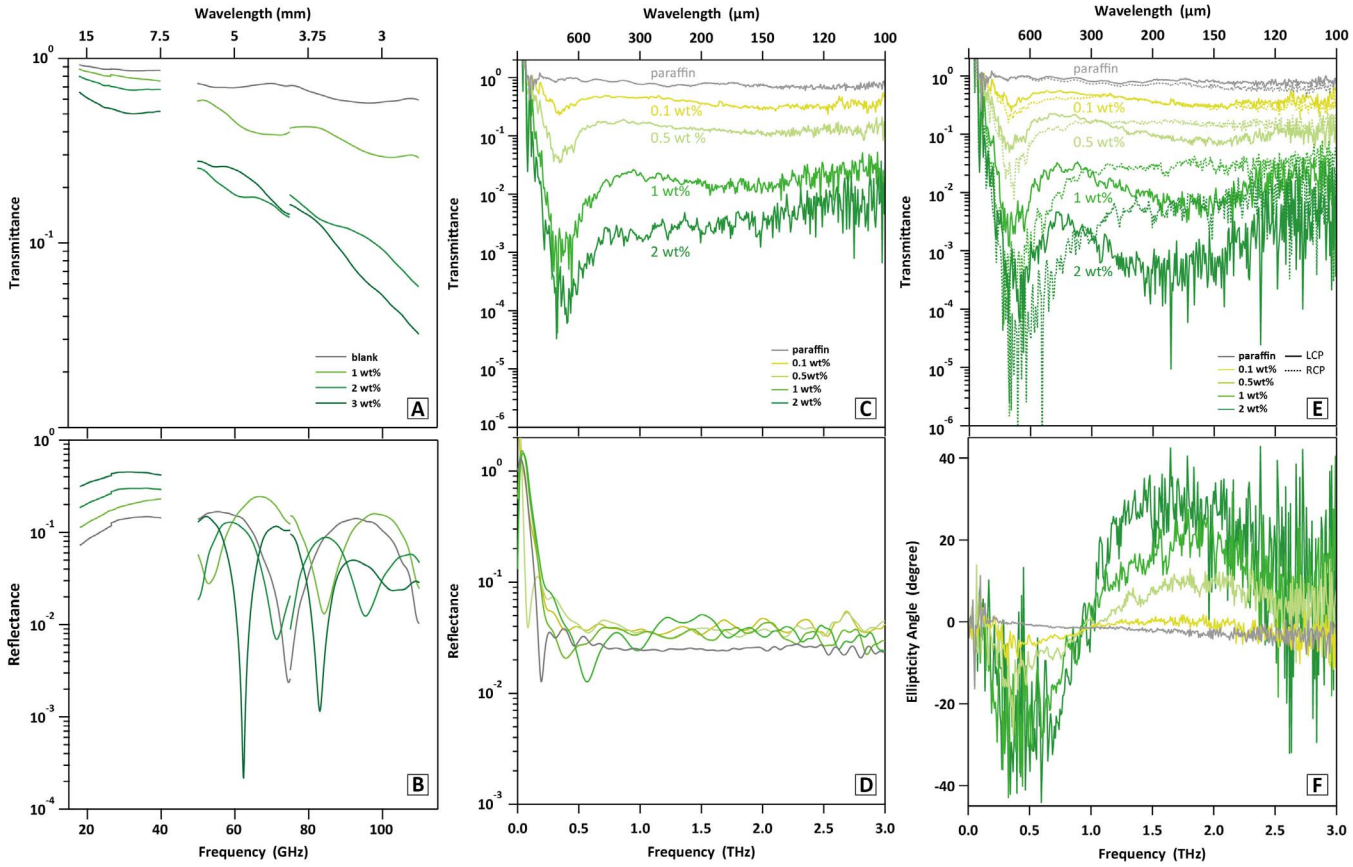

Figure 4 | Electromagnetic response of copper μcoil sheets. (a), (b) Transmission and reflection spectra in the region of 18–40 GHz and 50–110 GHz with a prescribed amount of μcoils in paraffin and silicon matrix, respectively. (c), (d) THz transmission and reflection spectra of LH μcoil-1 using non-polarization mode. The concentration dependence was evaluated with four different wt% (0.1, 0.5, 1, and 2 wt%, colored with pale to dark green). (e), (f) THz transmission spectra under circular polarization mode and their ellipticity angle spectra. Those of a μcoil-free paraffin sheet (gray line) are also depicted as reference. LCP (solid line) and RCP (dotted line) show transmittances against left-handed and right-handed circular polarizations, respectively.

concentration change in the region of V-band and W-band (50 to 110 GHz), although multi-reflections based on the sheet thickness were observed in every sample. The sheet showed remarkable transmission loss possibly based on absorption, for example, less than 10% transmittance at 60 GHz in case of 3 wt%. A monotonous decrease in transmittance at higher frequency region led us to realize resonance specific to the μcoil structure in the region of THz wave. THz time-domain spectroscopy (THz-TDS) with non-polarization mode was measured with the LH μcoil-1 dispersed into paraffin (Fig. 4c and 4d). No spectral feature with negligible reflection loss was observed in the μcoil-free paraffin sheet. Considerable transmission loss was observed over the entire region from 0.2 to 3.0 THz for the paraffin sheets containing only small amount (~2 wt%) of the LH μcoil. The μcoil concentration showed linear relationship to optical density converted from the transmittance, which is consistent with Lambert-Beer law (Fig. S19). The concentration dependence proved no anomalous radiation from imperfect dispersibility of μcoils. Furthermore, reflectance of the sheet was around 3%, so that the transmission loss was attributed to absorption of THz wave (for the spectra of all the LH μcoils with non-polarization mode, see Fig. S20). In order to evaluate optical activity of μcoil, THz-TDS combined with polarimetric analysis (THz-TDS-PA, SI-VII)[16,17] was conducted with the same sample, LH μcoil-1. Significant difference was found in transmittances against RH and LH circular polarizations (Fig 4e). The spectrum of ellipticity angle gave negative and positive bands in around 0.5 and 1.5 THz, respectively (Fig. 4f). The spectroscopic evidences supported that the μcoil-dispersion sheet exhibits optically active THz response. Here, we considered function of the structure handedness of LH μcoil for the optical activity found in the isotropic dispersion, unlike metal helix array[18,19]. Chigrin et al.[20] reported that achiral microparts can even effectively exhibit elliptical dichroism only based on their twisted configuration.

The LH and RH μcoils are optically active isomers. The variety of μcoils fabricated through systematic control of helical structures of *Spirulina* biotemplates enables us to experimentally evaluate structure-specific chiral electromagnetic responses. As references, it was confirmed that the dispersion sheets containing the straight copper wire and freeze-dried LH template-2 showed optical inactive. All of LH μcoils gave the similar spectral features of their ellipticities as the LH μcoil-1, *i.e.*, negative sign at 0.5 THz and positive one above 1.0 THz (Fig. 5a). At the same peak frequencies, the RH μcoils exhibited opposite signs of ellipticities (Fig. 5b). The LH μcoil-4 and RH μcoil-1 were selected here as enantiomeric pair with similar L_{free}/N values. The ellipticities of the enantiomeric pair obviously showed mirror-image spectra with opposite signs; +15° for LH μcoil-4, -10° for RH μcoil-1 at 2.0 THz (Fig. 5c). Separately, another sheet containing a racemic mixture of LH and RH μcoils with 1 wt% each traced the average of individual ellipticity angle spectrum, meaning no peaks with flat spectral feature (Fig. S21). The frequency showing sign inversion in ellipticity angle spectrum resulted in peak of rotation angle (Fig. S22). Therefore, it came to light that the LH μcoil emits the RH elliptical polarization and vice versa above the sign inversion frequency. That is to say, the LH μcoil shows dextrorotation and the RH one does levorotation.

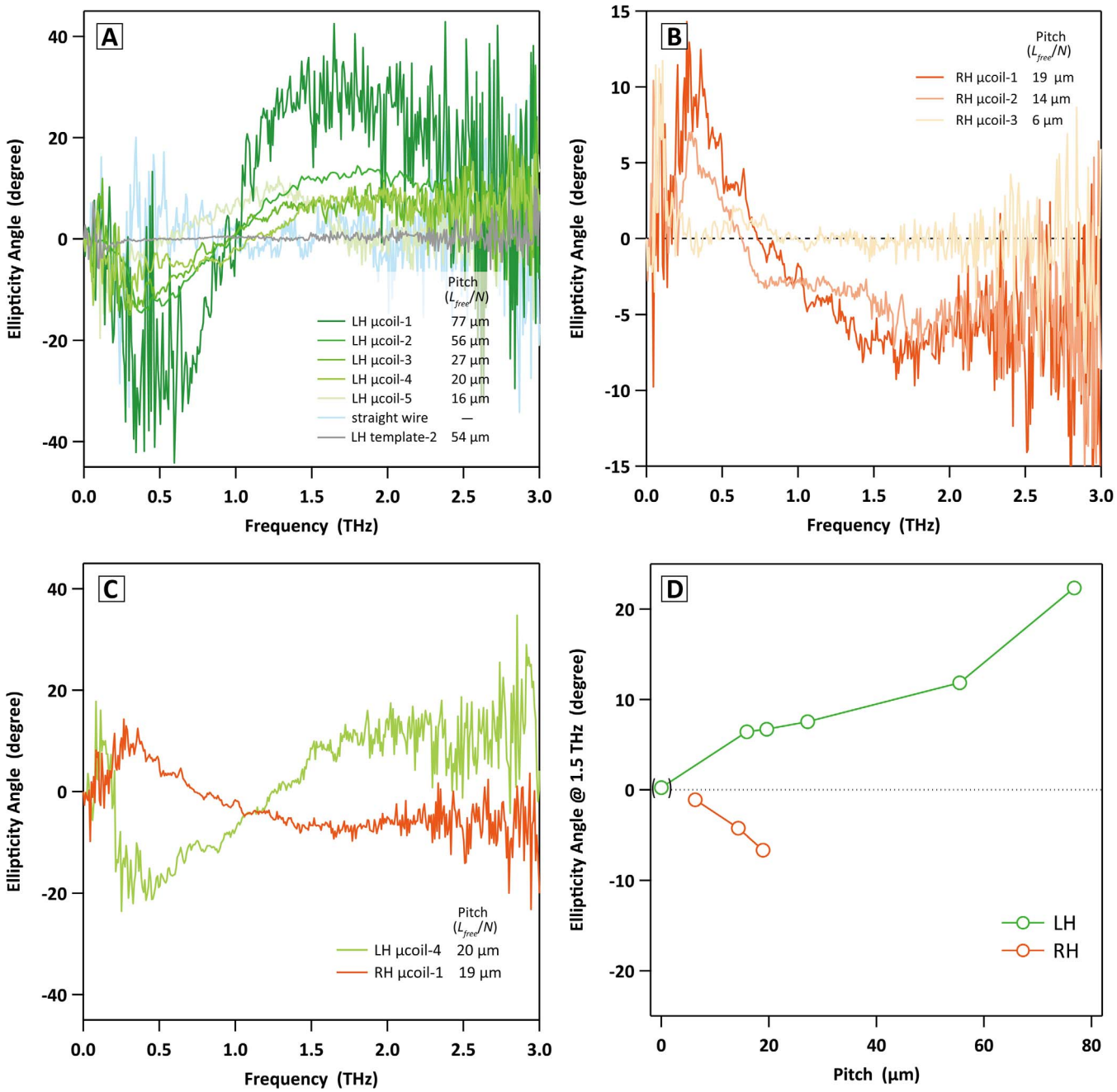

Figure 5 | Dependence of helical shape and handedness of µcoil on optically active response. (a), (b) Ellipticity angle spectra of µcoil-dispersion paraffin sheets were summarized into series of LH µcoils and RH µcoils as well as reference samples. All of samples contained 2 wt% in the paraffin matrices. The coil numbers and their L_{free}/N values are depicted in insets. The RH µcoil shows laevorotation with ellipticity angle of opposite sign against the LH case. The intensity of ellipticity angle decreased and also the inversion frequency, where occurs the sign inversion from negative to positive for LH µcoil and opposite inversion for RH µcoil, shifted toward lower frequency region as the L_{free}/N became smaller. Dispersion sheets of straight copper wire and freeze-dried LH template-2 with 54 µm in L_{free}/N showed no spectral features, which ensures the optical activity specific to the metal helical microstructure. (c) Ellipticity angle spectra of LH µcoil-4 and RH µcoil-1 selected as enantiomeric pair. (d) Ellipticity angle at 1.5 THz as a function of L_{free}/N. The value from the straight copper wire was depicted with parenthesis at 0 µm in pitch.

Discussion

There are three points of view to discuss the THz response observed in this study; the functional frequency region for µcoil response, the frequency at 0 ° of ellipticity angle (sign inversion frequency), the degree of ellipticity angle. First, the peak of ellipticity angle at higher frequency showed a tendency to shift inversely proportionally to length of wire to make one pitch, L_{wire}/N. The relationship between the L_{wire}/N and the functional frequency has been well explained by helical antenna theory[21] and helix array system[22], whose resonant wavelength is defined as $L_{wire}/N < \lambda < 2\ L_{wire}/N$. Briefly, it can be said that the µcoil sheet operates in a half-wave resonance mode ($\lambda = 2\ L_{wire}/N$) (Table 1 and SI-VIII). In the lower frequency region, the correlation specific to the structure was not observed. The possible reason is that there are many other resonance modes such as dipole mode, internal resonance based on L_{free}/N, and inter-coil coupling. Second, the sign inversion frequency shifted toward lower frequency as the sample was varied from loose to tight µcoils, which appeared closely related to the α. The sign inversion shift observed here was

found as having dominant self-resonant frequency, f_0, expressed with inductance, L, and capacitance, C, *i.e.*, $f_0 = \frac{1}{2\pi\sqrt{LC}}$. Since the tight μcoil has the shorter L_{free}/N as well as the larger N and/or D, the LC value should be larger, consequently giving the lower f_0. Finally, as a crucial sense, the intensities of ellipticities decreased as the L_{free}/N became smaller, in common with both of LH and RH μcoils (Fig. 5d). It has been reported that the helix array theoretically shows the same phenomenon[22]. In an extreme case, a ring or wire shape having $L_{free}/N = 0$ or $\alpha = 90$ °, respectively, loses chirality. We are also considering a similarity between the THz chiral behavior of μcoil and exciton chirality of optically active molecule. Similar to Davydov splitting in molecular crystal, an interactive pair of dipole moments induced by electric or magnetic field change along the helix causes the resonance energy split into two. Due to their twisted configuration, both resonances are allowed and act asymmetrically electromagnetic induction, resulting in the ellipticities with opposite signs. Further discussion on the optical activity with helical antenna response is under investigation. The alignment control in the sheet may allow us to fully understand the THz responses in our system.

The biotemplating process was successfully demonstrated to develop a new class of 3D-structured material. The *Spirulina*-based μcoil exhibited the optical activity, of which the conditions such as the sense of wave rotation and the operation frequency were controlled by the structural parameters of μcoils. A wide distribution on the structural parameters, always attendant on the biotemplating process, would be rather effective for broadband operation. The present fabrication process can be applied for various distinctive biological tissues and microorganism with mass-productivity and a wide variety of material form, which will promise new strategy for material design.

Methods

***Spirulina* cultivation and shape control.** The LH *Spirulina* (NIES-39 and -46, stock strains in National Institute for Environmental Studies) was cultivated with conventional aqueous media[10] in an open-air water tank at room temperature under fluorescent light (2,500 lx). For the shape control of *Spirulina* template, the cultivation temperature and light intensity were raised up to 35 °C and 7,500 lx, respectively. The LH template-1 was obtained from the standard condition and the LH template-2 to -5 were collected every fourth day from the mass cultivation medium with the controlled condition under way into the tightening of helix, decreasing of L_{free}/N. The linear strain was prepared by pure cultivation of the single trichome occurred by longer cultivation at the constant condition for more than 2 months.

Biotemplate process. The *Spirulina* was collected by a nylon mesh filter with 355 mesh and resuspended into a 100 mL of phosphate buffer solution (pH = 7.0) including 4% glutaraldehyde as tissue fixation solution. The optical density of the *Spirulina* suspension was adjusted to be around 2.0 at 550 nm with an optical pass length of 1 cm, which closely equals to the order of 10^5 in the number of *Spirulina* per 1 mL. The suspensions were left in ambient atmosphere overnight to complete fixation of *Spirulina* tissues. For further storage, they are kept in cool dark place so that the *Spirulina* can preserve their shapes and be used as the biotemplates for several years. Copper electroless plating onto the surface of *Spirulina* was conducted by the use of commercial products from Okuno Chemical Industries Co., Ltd.: for delipidation treatment, OPC-370 Condiclean MA; for Pd catalyzation (adsorption of Pd chloride based alkaline ionic catalyst), OPC-50 Inducer; for activation of the catalyst (reduction of Pd ion by dimethylamine borane), OPC-150 Cryster MU; for copper electroless plating, OIC Copper. All kinds of plating baths were initially prepared for 1 L. The preparation of plating baths and each processing time were listed in Table S1. A 20 mL of fixed *Spirulina* suspension was filtered with the nylon mesh to collect the number of *Spirulina* with 2×10^6, corresponding to 12 mg in weight of dried *Spirulina* and 200 cm^2/L in bath load. It is noted that the surface area of one *Spirulina* is typically around 1×10^4 cm^2. The *Spirulina* collected on the filter was immediately added to the baths before started to dry and stirred by mechanical stirrer with 300 rpm. The filtration and rinsing with water were successively carried out to switch the bath. After the final step with OIC Copper, the resulting copper μcoils were washed well on the filter and dispersed into 100 mL of distilled water overnight. The μcoils were collected by vacuum filtration using membrane filter (0.8-μm pore size, ATTP type, Isopore™ Track-Etched Membrane Filters) and dried in the atmosphere. The amount of μcoil generally averaged 90 mg, which gave 80% yield in the case of μcoil having 550 nm in the thickness of copper layer.

1. Bensaude-Vincent, B., Arribart, H., Bouligand, Y. & Sanchez, C. Chemists and the school of nature. *New J. Chem.* **1**, 1–5 (2002).
2. Sanchez, C., Arribart, H., Madeleine, M. & Guille, G. Biomimetism and bioinspiration as tools for the design of innovative materials and systems. *Nature Materials* **4**, 277–288 (2005).
3. Jin, M. H. *et al.* Superhydrophobic aligned polystyrene nanotube films with high adhesive force. *Adv. Mater.* **17**, 1977–1981 (2005).
4. Ishii, D., Yabu, H. & Shimomura, M. Novel biomimetic surface based on a self-organized metal−polymer hybrid structure. *Chem. Mater.* **9**, 1799–1801 (2009).
5. Kamata, K. *et al.* Fabrication of left-handed metal microcoil from spiral vessel of vascular plant. *Adv. Mater.* **23**, 5509–5513 (2011).
6. Vonshak, A. *Spirulina Platensis Arthrospira: Physiology, Cell-Biology And Biotechnology* (CRC Press, Bristol, PA, 1997).
7. Baurain, D. *et al.* Remarkable conservation of internally transcribed spacer sequences of *Arthrospira* ("*Spirulina*") (cyanophyceae, cyanobacteria) strains from four continents and of recent and 30-year-old dried samples from Africa. *J. Phycol.* **38**, 384–393 (2002).
8. Zafaralla, M. T. *et al.* Protein from *Spirulina*. *NSTA Technol. J.* **10**, 18–26 (1985).
9. Chen, B., Zhan, T., Lian, Z. & Zhang, D. Magnetization of microorganism cells by sol-gel method. *Sci. in China Ser. E: Technol. Sci.* **51**, 591–597 (2008).
10. Ogawa, T. & Terui, G. Growth kinetics of *Spirulina platensis* in autotrophic and mixotrophic cultures. *Ferment. Technol. Today, Proc. Int. Ferment. Symp. 4th*, 543–549 (1972).
11. Ma, Z. & Gao, K. Photoregulation of morphological structure and its physiological relevance in the cyanobacterium *Arthrospira* (*Spirulina*) *platensis*. *Planta* **230**, 329–337 (2009).
12. Ishii, D. *et al.* Pd-Promoted Ni-P Electroless Deposition on a Hydrogen-Bonded Molecular Surface of a Supramolecular Fibrous Template. *Chem. Mater.* **18**, 2152–2158 (2006).
13. Bockris, J. O. M., Reddy, A. K. N. & Gamboa-Aldeco, M. E. *Modern Electrochemistry 2A: Fundamentals of Electrodics, Electrodics* Ch. 7, 1035–1400 (Kluwer Academic/Plenum Publishers, 2000).
14. Migneault, I., Dartiguenave, C., Bertrand, M. J. & Waldron, K. C. Glutaraldehyde: behavior in aqueous solution, reaction with proteins, and application to enzyme crosslinking. *BioTechniques* **37**, 790–802 (2004).
15. Mühling, M., Harris, N., Belay, A. & Whitton, B. A. Reversal of helix orientation in the vyanobacterium *Arthrospira*. *J. Phycol.* **39**, 360–367 (2003).
16. Hangyo, M. & Takano, K. Metamaterials for terahertz waves. *Mater. Integr.* **24**, 13–20 (2011).
17. Hangyo, M., Tani, M. & Nagashima, T. Terahertz time-domain spectroscopy of solids: a review. *Int. J. Infrared millimeter Waves* **26**, 1661–1690 (2005).
18. Gansel, J. K. *et al.* Gold helix photonic metamaterial as broadband circular polarizer. *Science* **325**, 1513–1515 (2009).
19. Yu, Y., Yang, Z., Zhao, M. & Lu, P. Broadband optical circular polarizations in the terahertz region using helical metamaterials. *J. Opt.* **13**, 055104 (2011).
20. Chigrin, D. N., Kremers, C. & Zhukovsky, S. V. Plasmonic nanoparticle monomers and dimers: from nanoantennas to chiral metamaterials. *Appl. Phys. B* **105**, 81–97 (2011).
21. Balanis, C. A. *Antenna Theory: Analysis and Design* (Wiley, New Jersey, 2005).
22. Li, S., Yang, Z. Y., Wang, J. & Zhao, M. Broadband terahertz circular polarizers with single- and double-helical array metamaterials. *J. Opt. Soc. Am. A* **28**, 19–23 (2011).

Acknowledgments

This work was partly supported by MEXT KAKENHI, Grant-in-Aid for Scientific Research on Innovative Areas (22109006) and for Challenging Exploratory Research (22651051). Okuno Chemical Industries Co., LTD. provided electroless plating baths. The authors acknowledge Y. Akimoto and S. Hirashima for their support on SEM observations, and T. Nojima for helpful discussions. K.K. thanks T. Tadokoro for his invaluable comments about definition of circular polarization.

Author contributions

K.K., S.S., A.Y. and T.I. started this project; T.F. and W.T. contributed to the design of experiment; Z.P., M.I., S.H. and A.B. conducted *Spirulina* cultivation; K.T. and M.H. performed the THz-TDS and data analysis; T.I. and M.H. coordinated the study with contributions from T.H., T.T. and K.N.; K.K. wrote the manuscript.

Additional information

Supplementary information accompanies this paper at http://www.nature.com/scientificreports

Competing financial interests: The authors declare no competing financial interests.

How to cite this article: Kamata, K. *et al.* *Spirulina*-Templated Metal Microcoils with Controlled Helical Structures for THz Electromagnetic Responses. *Sci. Rep.* **4**, 4919; DOI:10.1038/srep04919 (2014).

Supplementary Information

Spirulina-Templated Metal Microcoils with Controlled Helical Structures for THz Electromagnetic Responses

Kaori Kamata, Zhenzi Piao, Soichiro Suzuki, Takahiro Fujimori, Wataru Tajiri, Keiji Nagai, Tomokazu Iyoda, Atsushi Yamada, Toshiaki Hayakawa, Mitsuteru Ishiwara, Satoshi Horaguchi, Amha Belay, Takuo Tanaka, Keisuke Takano, & Masanori Hangyo

Sections

SI-I. Symbols for the structural parameters of microcoil (μcoil)

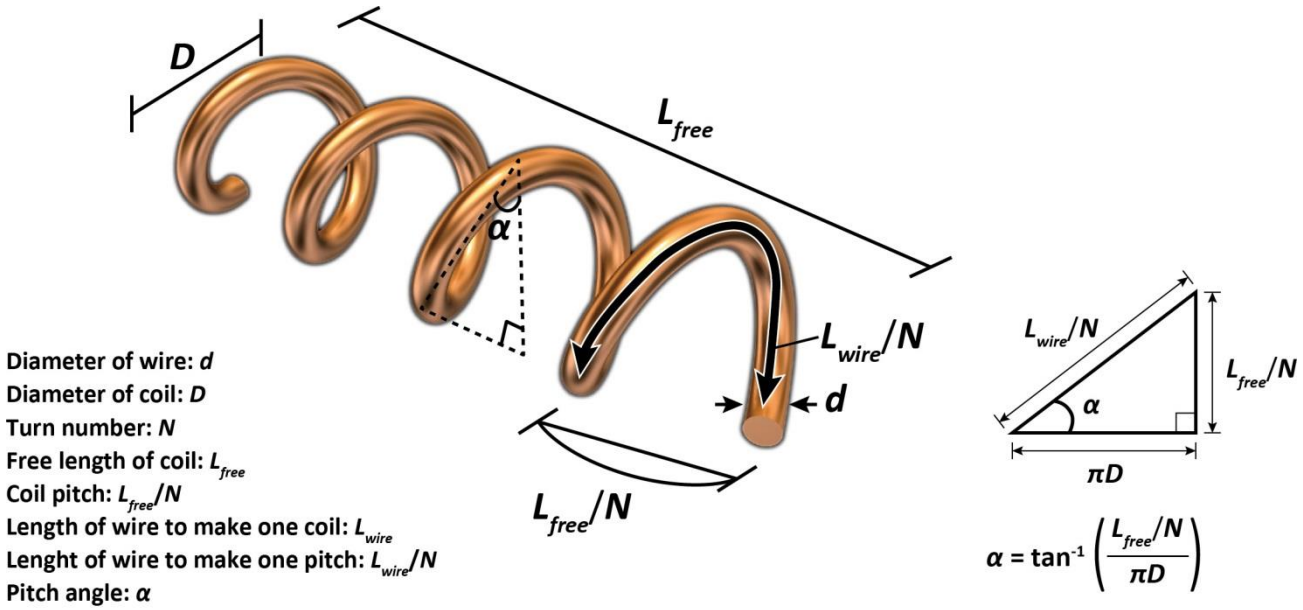

Figure S1 Symbols for the structural parameters of μcoil.

SI-II. Culture condition and structure observation of *Spirulina*

Spirulina, a blue-green algae in natural helical shape, were obtained by division from National Institute for Environmental Studies. The strain we used for the standard biotemplate was NIES-39, originally came from Lake Chad in Central African Republic, while for control of helical pitch, we selected NIES-46, from Lake Texcoco, due to its controllability on the helical structure under the different conditions of cultivation. Both of the strains have left-handed (LH) helix structure. The *Spirulina* was propagated in SOT (*Spirulina* Ogawa-Terui) medium at different environmental factors, temperature and light intensity. It has been known that physical and chemical conditions may affect the helix geometry (ref. 11 in the main text). At room temperature under fluorescent light irradiation with 2500 lx in our lab., the number of *Spirulina* doubles in a day, so that we are doing the routine cultivation from 10^2 to 10^5 in the *Spirulina* concentration (mL^{-1}) for almost one week. The growth curve was well fitted with an exponential function, *i.e.*, $y = N_0 \exp(ax)$, where the N_0 is the initial concentration of *Spirulina* and a is coefficient (Fig. S2). By optical microscopy (Olympus, BX51), the wire diameter (d), diameter of helix (D), pitch (L_{free}/N), turn number (N), free length (L_{free}), and pitch angle (α) of *Spirulina* (NIES-46) are found as approximately 6 μm, 43 μm, 74 μm, 2.4, 174 μm,

and 29 °, respectively (Fig. S3A-D). The culture temperature and light intensity were raised to 35 °C and 7500 lx, respectively, but the other factors were fixed. After the cell growth became stationary, the structural parameters were observed. It was found that the culture at 35 °C under the stronger intensity of light produced tight helix with L_{free}/N = 16 μm drastically smaller than the case at room temperature. In order to obtain the intermediate L_{free}/N between 77 and 16 μm, sampling approach was carried out by collecting *Spirulina* from the mass cultivation medium before the helix shape became stationary. Here, five different LH *Spirulina* having 77 μm, 55 μm, 27 μm, 20 μm, 16 μm in L_{free}/N were prepared as biotemplates, which were numbered as LH template-1 to -5. The LH template-2 was originated from the strain of NIES-39, the others were from the same strain as NIES-46.

Such flexible morphologies in the *Spirulina* offer many advantages on the fabrication of μcoils, which could show wide range of electromagnetic applications based on their controlled structural parameters.

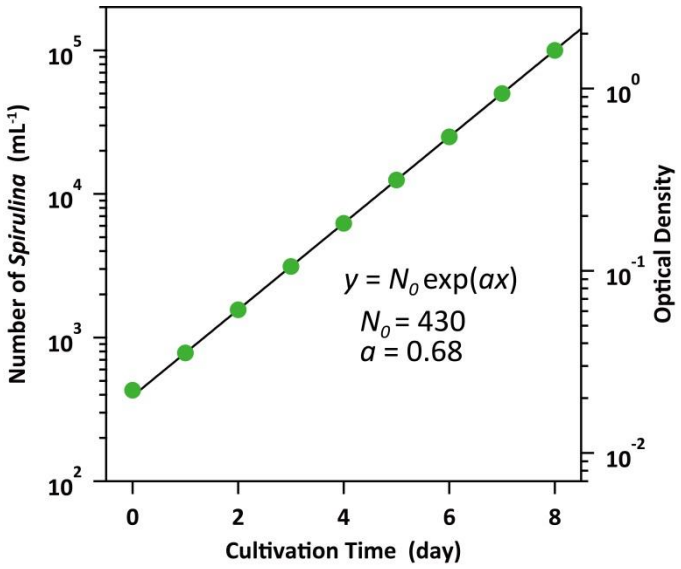

Figure S2 Growth curve of *Spirulina* under the regular cultivation condition. The number of *Spirulina* (dot) in 1 mL of cultivation medium was plotted as a function of cultivation time in logarithmic scale. Initial *Spirulina* concentration was 430 mL^{-1}. For the data collections, the number of *Spirulina* in 10 μL was counted under the optical microscope after dilution of the *Spirulina* suspension with water by 100 times. The growth curve well follows the exponential function (solid line). Experimentally, we monitored the optical density to estimate the *Spirulina* concentration.

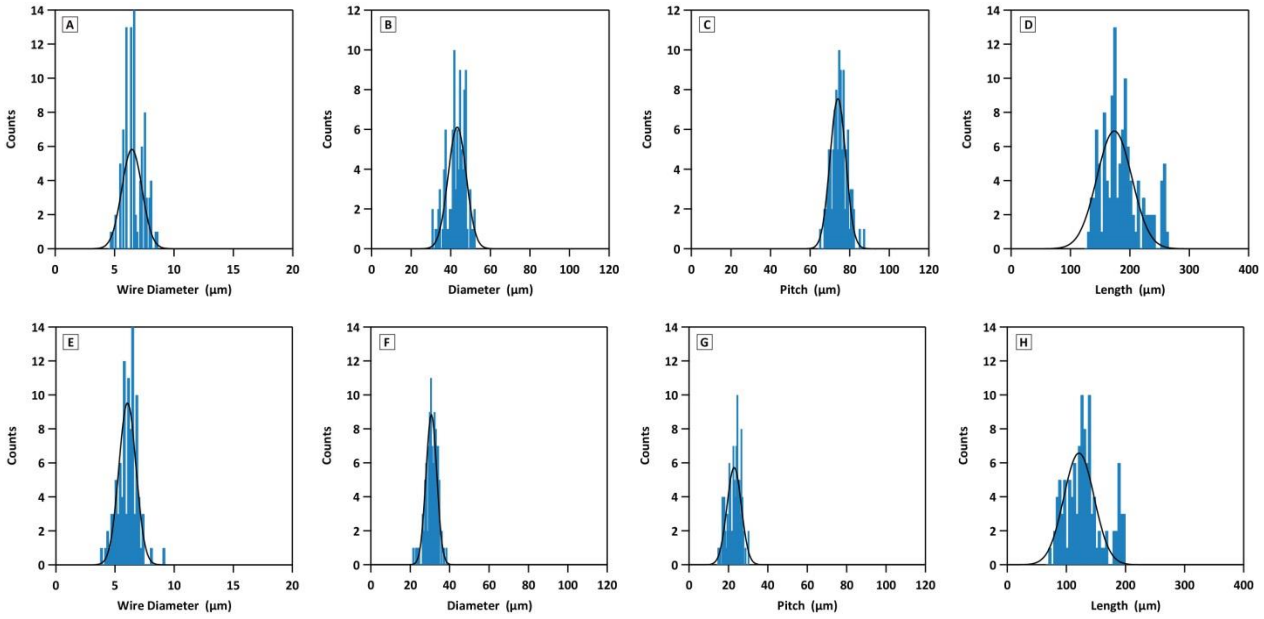

Figure S3 Histograms of structural parameters on helix geometries of *Spirulina*. (A), (E) Wire diameter (d), (B), (F) coil diameter (D), (C), (G) coil pitch (L_{free}/N), and (D), (H) free length of coil (L_{free}) were evaluated for the *Spirulina* LH template-1 and RH template-1, cultivated at room temperature with 2000 lx in light intensity. The black lines indicate Gaussian distributions to have averaged values. The structural parameters and percent relative standard deviations (%RSD) for the LH template-1 (A-D) are found as; d = 6 μm (13 %), D = 43 μm (11 %), L_{free}/N = 74 μm (5 %), L_{free} = 174 μm (17 %), for the RH template-1 (E-H), d = 6.1 μm (12 %), D = 31 μm (9 %), L_{free}/N = 23 μm (16 %), N = 7, and L_{free} = 121 μm (21 %).

We have failed to find RH *Spirulina*, although various cultivation conditions were tried. As mentioned in the main text, to search the naturally alive RH *Spirulina* became the possible candidate. A strain of RH *Spirulina* was obtained from Earthrise Nutritionals, LLC, a wholly owned subsidiary of DIC Corporation. One piece of RH *Spirulina* was picked up and transferred to cultivation medium for the pure cultivation. It took almost one month to have 1 L of cultivation medium with almost 10^5 mL^{-1} in concentration of RH *Spirulina*. The structural parameters of typical RH *Spirulina* (RH template-1) and their %RSDs were observed as d = 6.1 μm (12 %), D = 31 μm (9 %), L_{free}/N = 23 μm (16 %), N = 7, and L_{free} = 121 μm (21 %) (Fig. S3E-H). The L_{free}/N of RH *Spirulina* was controlled in a similar manner to the way of LH case for the preparation of RH template-1 to -3.

SI-III. *Spirulina*-based biotemplating process

Table S1 Procedure on Cu μcoil fabrication via electroless plating**.**

Process	Reagent	concentration	temperature	treatment time
(i) Fixation	glutaraldehyde	4 %	r.t.	over night
↓				
(ii) Pd catalyzation				
Delipidation	OPC-370 Condiclean MA	50 ml/L	40 °C	5 min
↓ filtration and washing				
		(pH 12)		
Pd catalyzation	OPC-50 Inducer A (30 mmol/L Pd ion)	25 ml/L	40 °C	5 min
	OPC-50 Inducer C	25 ml/L		
↓ filtration and washing				
Activation (reduction of Pd ion)	OPC-150 Cryster MU	75 ml/L	25 °C	5 min
↓ filtration and washing				
(iii) Cu electroless plating	OIC Copper 1 (0.6 mol/L Cu ion)	20 ml/L	40 °C	10 min
	OIC Copper 2	9 ml/L		
	OIC Copper 4	100 ml/L		
↓ -filtration and washing -stored in water overnight -filtration and drying				
Cu μcoil				

Each electroless plating bath was prepared for 1 L including prescribed amount of each plating reagent listed in Table S1. It is noted that the bath for Pd catalyzation and Cu electroless plating were prepared to include Pd ion with 0.8 mmol/L and Cu ion with 20 mmol/L, respectively. The amount of fixed *Spirulina* suspension in phosphate buffer solution with 4 % glutaraldehyde can be varied up to 40 mL, meaning that the total surface area of *Spirulina* against the volume of plating bath is limited to 400 cm^2/L. Higher total surface area resulted in strong entanglement and aggregation and also imperfect Cu coating on the *Spirulina* surface.

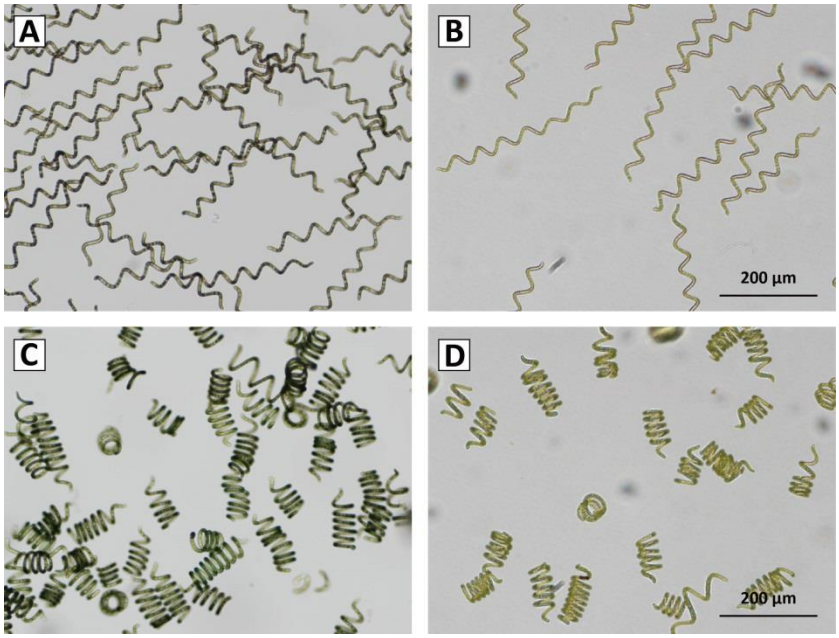

Figure S4 Optical micrographs of LH template-2 (A, B) and LH template-5 (C, D) at different stage of biotemplating process; A and C, after the fixation with glutaraldehyde; B and D, after the activation process reducing Pd ion adsorbed to *Spirulina*.

Characterization of Pd catalyst nuclei adsorbed to *Spirulina*.

The shape preservation of *Spirulina* templates was ensured after fixation with glutaraldehyde and also after pretreatment, the activation process of Pd catalyst (Fig. S4). The Pd-based catalyst nuclei adsorbed to the *Spirulina* indicated in Fig. S4B were characterized by X-ray photoelectron spectroscopy (XPS, Shimadzu, ESCA-3400) as forming metallic Pd with the content of 86 % and a little amount of oxides (PdO_x) (Fig. S5). The experimental curve in the Pd 3*d* region was fitted with Gauss function at the already-identified Pd $3d_{5/2}$ and Pd $3d_{3/2}$ peak positions[1]. The Pd 3*d* doublet appeared at 340.7 and 335.4 eV was reasonably assigned to metallic Pd with the expected intensity ratio of 1.5 and the other doublet at 338.0 and 343.3 eV was assigned to electron-deficient Pd normally described as PdO_x. The intensity ratio of peaks for metallic Pd and PdO_x in the Pd $3d_{5/2}$ range was 6.15, leading to that 86 % of Pd content was metallic.

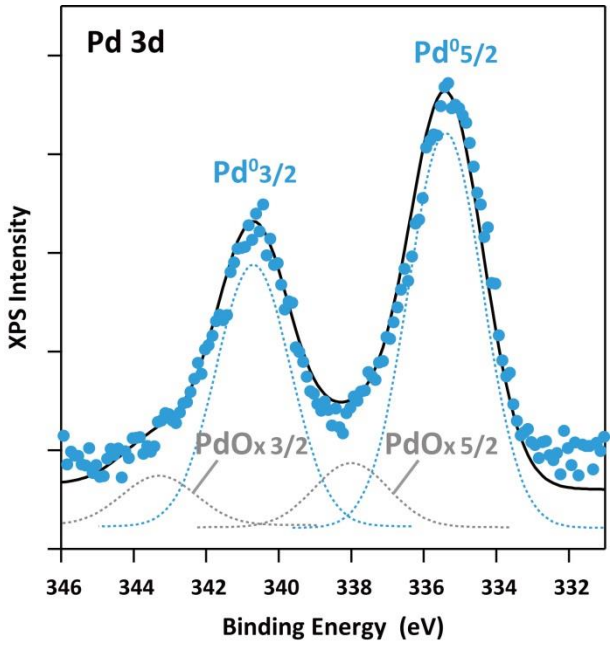

Figure S5 Pd 3*d* XPS profile of *Spirulina*, LH-template 2, after the activation in the biotemplating process; blue dot, measured intensity: black solid line, Gaussian curve given by multi-peak fitting; dotted line, individual peaks identified as Pd metal and PdO_x in the $3d_{5/2}$ and $3d_{3/2}$ ranges.

Table S1 Quantitative analyses of Pd content adsorbed into the *Spirulina* template.

Samples	**Pd treatment** (min)	**ICP results: Pd content per one *Spirulina***			
		(g)	(mol)	(m^3)	(vol %)[*1]
LH-template 2	1	0.4×10^{-9}	3.3×10^{-12}	0.03×10^{-15}	0.5
	3	0.8×10^{-9}	7.3×10^{-12}	0.06×10^{-15}	1.1
	5	1.2×10^{-9}	12×10^{-12}	0.1×10^{-15}	1.7

*1: The **LH-template 2** has an average volume of one *Spirulina* as 6.0×10^{-15} m^3, so that the volume fractions of Pd content in vol% were obtained by the ICP-detected Pd volume divided by the volume of *Spirulina* template.

The inductively coupled plasma-optical emission spectrometry (ICP-OES, Shimadzu, ICPS-8100) revealed that the amount of Pd content in the *Spirulina* template was linearly increased as the Pd catalyzation step proceeded up to 5 min (Table S1 and Fig. S6A). The adsorption rate was found as 2.4×10^{-12} mol/min given by the slope of fitted line. The Pd content was finally adsorbed to the *Spirulina* template with 12×10^{-12} mol for one strain of *Spirulina*, which equals almost 2 vol % in volume fraction of Pd content per one *Spirulina*. It

was also found in observation of energy dispersive X-ray spectrometry (EDX, Oxford Instruments, Swift ED 3000) equipped with SEM (Hitachi, TM3000) that the Pd-based catalyst nuclei formed nanoparticles smaller than the resolution limit of SEM and the Pd nanoparticle was uniformly adsorbed on the surface of *Spirulina* template (Fig. S6B).

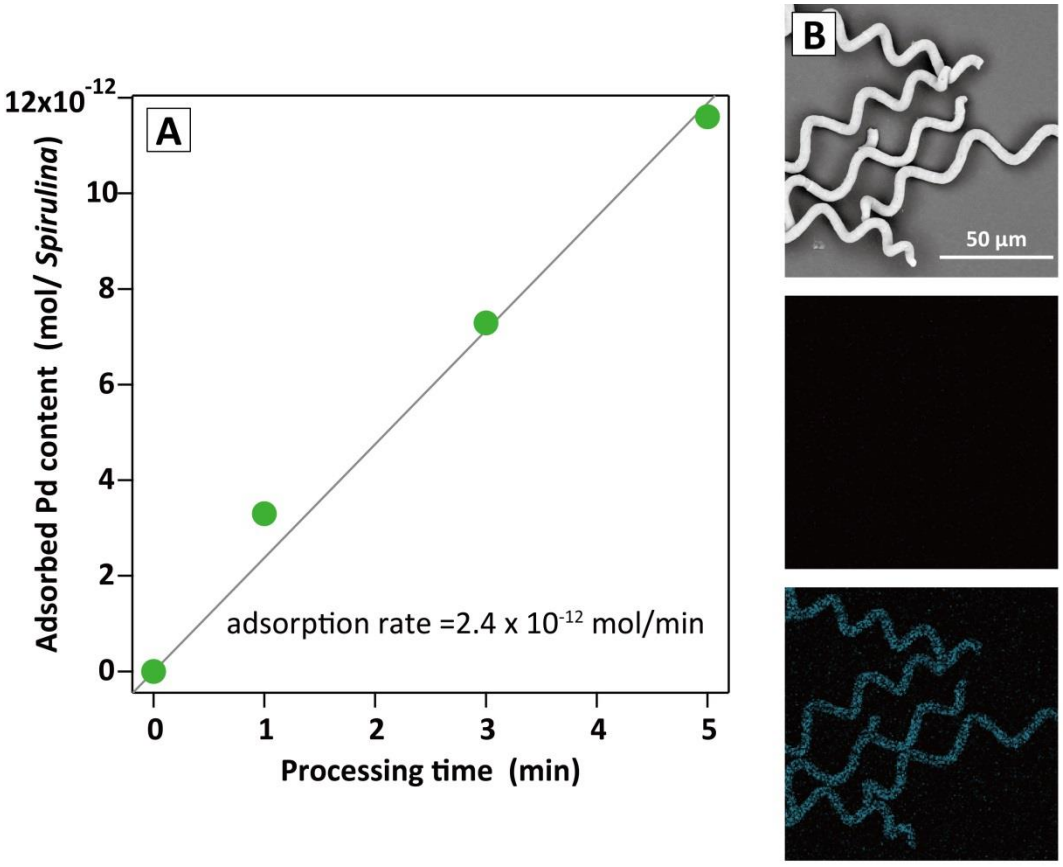

Figure S6 (A) The amount of Pd content per one strain of *Spirulina* (green dot) detected in ICP measurement as a function of treatment time for the Pd catalyzation using OPC-50 Inducer bath. The result was fitted by linear function (solid line) to derive the adsorption rate from the slope. The ICP measurements were carried out with the samples after the activation process (all for 5 min) using OPC-150 Cryster MU. (B) The EDX-SEM observation of *Spirulina* treated with 5-min Pd catalyzation and 5-min activation process: top, back-scattered electron image; middle, Cu Kα mapping; bottom, Pd Lα mapping.

The distribution of Pd catalyst nuclei in/on the *Spirulina* template was identified by EDX-SEM observation (Fig. S7). The Pd Lα mapping visualized the side surface as well as the cross-section formed in intentionally damaged for the observation of Pd distribution inside the

Spirulina. The line analysis was conducted across the cross-section, indicating that the intensity of Pd Lα became higher at the interface of *Spirulina* and kept constant towards a center of the cross-section. The Cu Kα intensity was weaker than the detection limit as a matter of course. It was found here that the Pd ion can be defused into the *Spirulina* tissue and the resulting Pd nanoparticle generated at the stage of activation are equally distributed to the surface and inside of *Spirulina*.

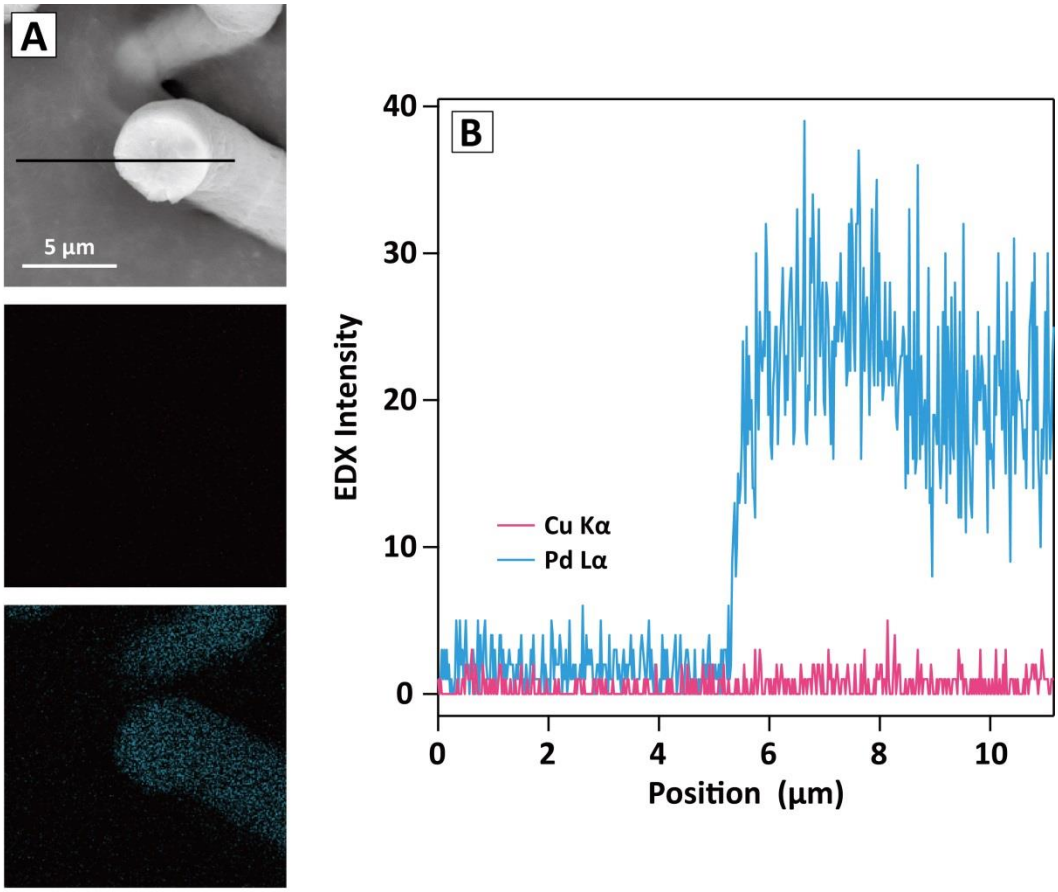

Figure S7 (A) The EDX-SEM observation with back-scattered electron image (top), Cu Kα (middle), and Pd Lα (bottom) mappings. (B) The line analyses for Cu Kα (pink line) and Pd Lα (blue line) across the line indicated in top image of (A), recorded from left to right. The cross-section of *Spirulina* after the activation was intentionally prepared by collapsing the sample on SEM stage with edge of spatula.

In order to confirm the distribution of Pd catalyst nuclei in the *Spirulina*, TEM observation (Jeol, JEM-2100) was employed by using the sample treated up to the activation step (Fig. S8). The sample was microtomed to the direction of long-axis of *Spirulina* without any staining.

The resulting thin-section was found as having contrast high enough to be visualized, indicating uniform distribution of Pd catalyst nuclei as a heavy metal into the *Spirulina*. It is noted that the cell wall as well as the outer membrane can be clearly observed without the staining.

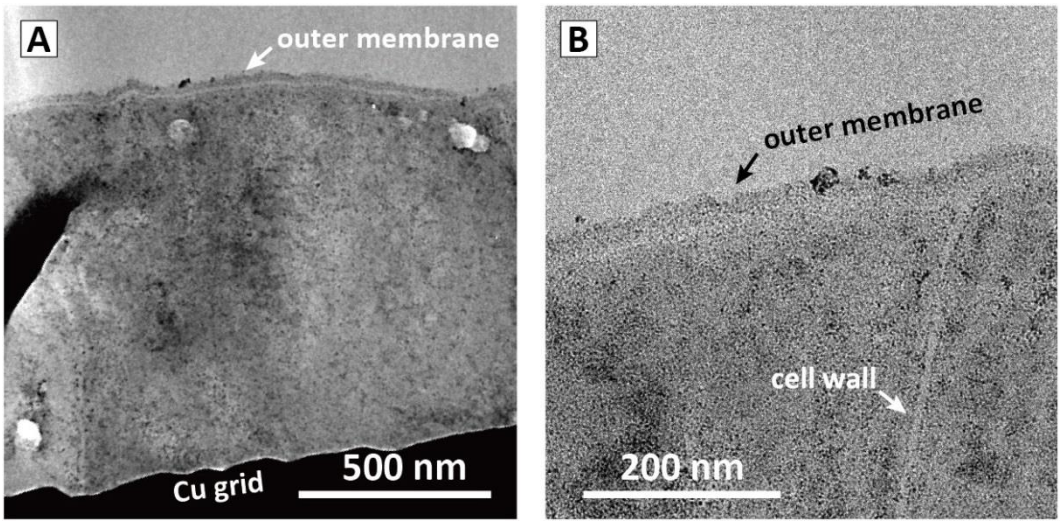

Figure S8 TEM images of thin-section of *Spirulina*. The image of (A) was obtained to show one cell of *Spirulina*, while the (B) was magnified image. The sample after the activation process was used and the staining was not carried out. The thin-section was prepared by microtoming to the direction of long-axis of *Spirulina*.

Copper electroless plating and characterization of product.

The Cu electroless plating was carried out onto the surface of *Spirulina* including the Pd catalyst nuclei as shown in Fig. S9. The Pd nanoparticles adsorbed on the surface can be the plating catalyst, since as the anodic reaction the Pd catalyst oxidizes the reducing reagent in OIC Copper plating bath to produce an electron under alkaline pH. The electron produced from the reducing reagent is consumed to reduce the Cu ion as cathodic reaction, leading to the formation of metallic Cu on the *Spirulina* surface. The resulting Cu on the outermost surface can work as self-catalyst to grow the Cu deposition layer. The XPS revealed that the Cu layer was consisting of metallic Cu (and/or cuprous oxide, Cu_2O, closely overlapped) and a little amount of cupric oxide, CuO (Fig. S10). The experimental curve in the Cu 2*p* region was fitted with Gaussian function at the already-identified Cu $2p_{3/2}$ and Cu $2p_{1/2}$ peak positions[2]. The Cu 2*p* doublet appeared at 932.27 and 952.05 eV was reasonably assigned to metallic Cu and/or Cu_2O with the expected intensity ratio of 2.0 and the other doublet at 934.44 and 953.84 eV was assigned to the CuO. The intensity ratio of peaks in the Cu $2p_{3/2}$ range was 8.7, leading to that 90 % of Cu content was metallic or Cu_2O. The X-ray powder diffraction (XRD, Rigaku RINT-Ultima) pattern gave two major peaks appeared at 43.3 and 50.4 degrees in 2 theta,

consistent with FCC-structured crystalline Cu (Fig. S11). The calculated lattice constants of the Cu μcoil are in good agreement with the standard literature values (JCPDS file No. 04-0836). The peak area of Cu metal was almost 25 times wider than that of Cu oxides. From the result, the deposited layer on the surface was mainly consisting of single phase of crystalline Cu metal with a little amount of oxidized Cu like CuO and Cu_2O.

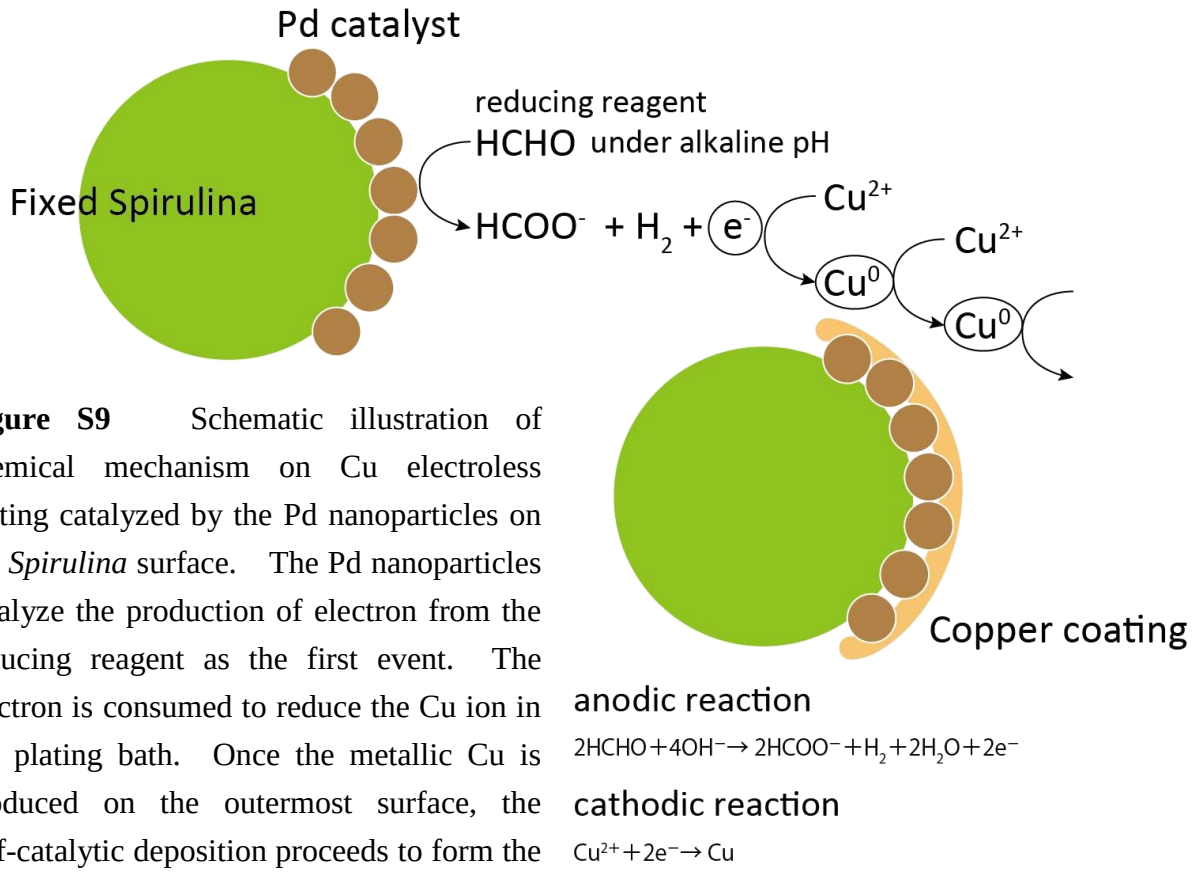

Figure S9 Schematic illustration of chemical mechanism on Cu electroless plating catalyzed by the Pd nanoparticles on the *Spirulina* surface. The Pd nanoparticles catalyze the production of electron from the reducing reagent as the first event. The electron is consumed to reduce the Cu ion in the plating bath. Once the metallic Cu is produced on the outermost surface, the self-catalytic deposition proceeds to form the Cu layer on the *Spirulina* surface.

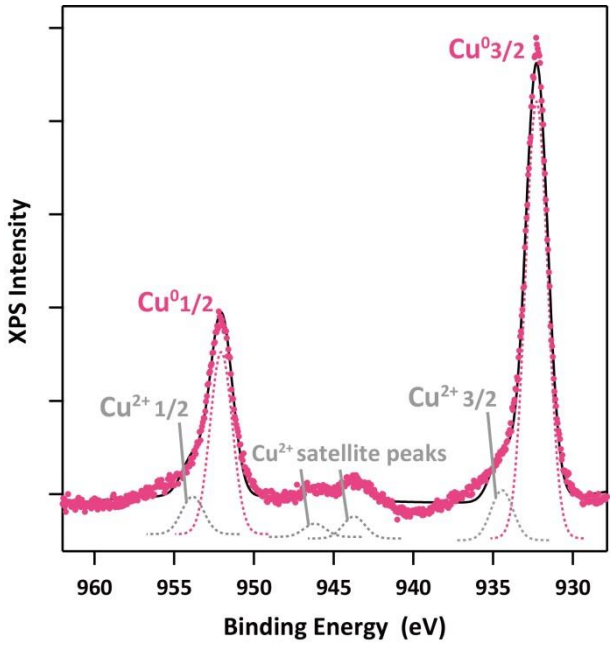

Figure S10 Cu 2*p* XPS profile of Cu μcoil, obtained through the electroless plating for 10 min.; pink dot, measured intensity; black solid line, Gaussian curve given by multi-peak fitting; dotted line, individual peaks identified as Cu metal (and/or closely overlapped Cu_2O) and CuO in the $2p_{3/2}$ and $2p_{1/2}$ ranges.

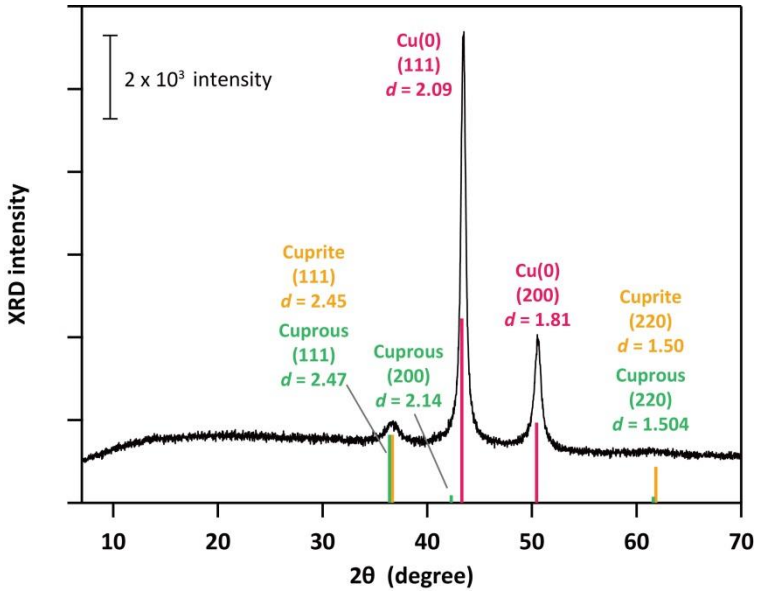

Figure S11 XRD pattern of Cu μcoil with the theoretical peak positions (sticks to zero), *d*-spacings, and crystalline phases of Cu metal and Cu oxides.

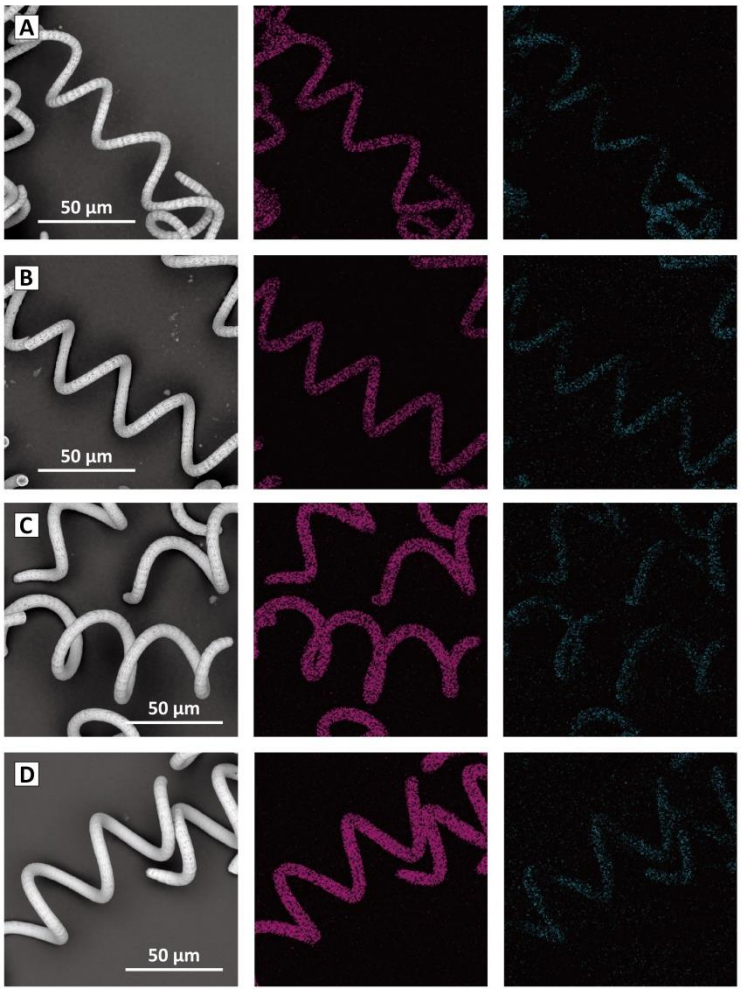

Figure S12 EDX-SEM observation of Cu µcoils obtained through the electroless plating up to 10 min.: left, back-scattered electron image; middle, Cu Kα mapping; right, Pd Lα mapping. The images were taken with the samples at different stage of electroless plating: (A), 2.5 min; (B), 5.0 min; (C), 7.5 min; (D), 10 min.

The EDX-SEM observations were examined to characterize the surface during the electroless plating (Fig. S12). The samples were collected from the plating bath at the different time, *i.e.*, 2.5, 5.0, 7.5, and 10 min. The back-scattered electron images showed higher contrast and the Cu Kα mapping visualized the microstructural feature of µcoils more clearly as the plating reaction proceeded. The Pd Lα mapping gave low contrast throughout the plating process. The EDX spectra indicates that intensities of peaks at 0.93 and 8.04 keV, corresponding to Cu Lα and Kα lines, respectively, increased as a function of plating time (Fig. S13), while an area of peak at 2.83 keV, assigned to Pd Lα, was relatively smaller.

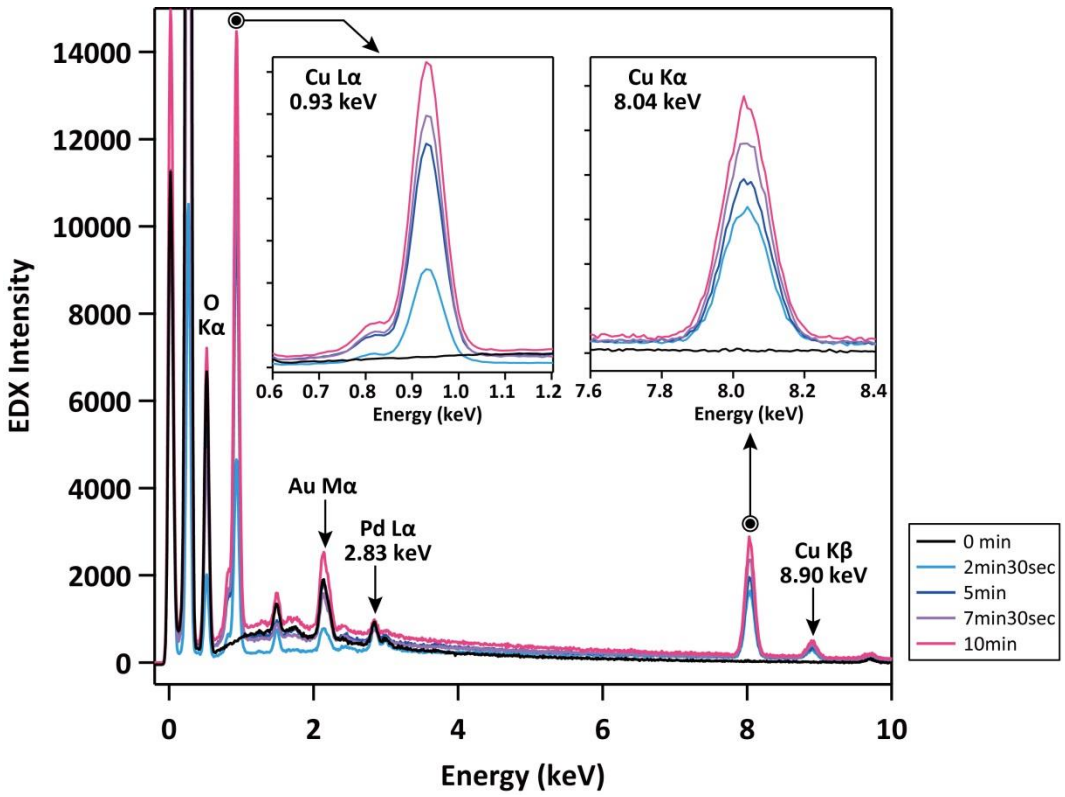

Figure S13 EDX spectra of Copper μcoils prepared at the different plating time. The sample was treated up to the activation process as described in Table S1and successively the electroless plating was conducted for prescribed time. The spectrum at 0 min was obtained from the sample just after the activation, so that only Pd nanoparticles were included in the sample. All the spectra were raw data without offset and normalization. The Au peak was detected because the Au spattering was used to avoid charge-up during the measurements.

SI-IV. Control of Copper layer thickness

In the electroless plating techniques, it has been known that there are several methods to control the thickness of deposited metal layer such as temperature or pH condition. But the loading amount of *Spirulina* suspension is most effective and easily varied in our study. The total surface area of sample against the volume of plating bath, namely, bath load, is essential for the thickness and continuous coating. In order to evaluate the appropriate loading amount for our system, efficiency of Cu deposition was obtained as follows. The efficiency was defined as the volume (m^3) of deposited Cu content to the surface area (S in m^2) of *Spirulina*, *i.e.*, average Cu layer thickness specific in the bath load. The surface are of one *Spirulina* can be derived by $S = \pi d L_{wire} + 2\pi(d/2)^2$. A 40 mL of the *Spirulina* suspension, totally including 4 x 10^6 in the number of *Spirulina*, gives the bath load of 400 cm^2/L, because the surface area of one *Spirulina* is typically in the order of 10^{-4} cm^2. Under this bath load, the Cu electroless plating

was examined and the samples were collected at the different plating time. The ICP analyses revealed that the Cu content increased to 0.31 x 10^{-9} mol (2.2 x 10^{-15} m^3 in the volume) per one *Spirulina* up to 10-min plating, while the Pd content was constant during the plating reaction (Table S2). From the ICP results, the deposition speed and efficiency were found as 22 nm/min and 220 nm, respectively. As double-check, the cross-section of Cu μcoil was observed by SEM (Fig. S14). The resulting μcoil had tubular structure with fixed *Spirulina* template inside as inclusion. It can be assumed that the cytoplasmic components after glutaraldehyde tissue fixation were preserved in the electroless plating bath, and the shape of *Spirulina* was effectively templated. The thickness evaluated from the SEM image was plotted as a function of plating time with the ICP results in Fig. S14. The deposition speed was estimated as 19 nm/min, slightly different from the ICP result. But it should be in allowable range, since the unevenness of plating layer and also the inherent size distribution of *Spirulina* template are considered. From the relationship between the bath load and efficiency, the thickness can be roughly predicted at the different bath load, since the thickness is inversely proportional to the bath load. The loading amount of *Spirulina* suspension with 20 mL was employed to be bath load of 200 cm^2/L in this study, leading to the average Cu layer thickness of 550 nm enough to exhibit bulk-like electric property (Fig. S15).

Table S2 Quantitative analyses of Pd and Cu contents adsorbed into/onto the *Spirulina* template during the electroless plating process

Samples	**Cu plating time** (min)	**ICP results: Pd content per one *Spirulina***			
		(g)	(mol)	(m^3)	(vol %)
LH-μcoil-2	2.5	0.59 x 10^{-9}	5.5 x 10^{-12}	0.049 x 10^{-15}	0.8
	5.0	0.55 x 10^{-9}	5.2 x 10^{-12}	0.046 x 10^{-15}	0.8
	7.5	0.62 x 10^{-9}	5.8 x 10^{-12}	0.051 x 10^{-15}	0.9
	10	0.62 x 10^{-9}	5.8 x 10^{-12}	0.052 x 10^{-15}	0.9

Samples	**Cu plating time** (min)	**ICP results: Cu content per one *Spirulina***			Deposition efficiency (nm) *1
		(g)	(mol)	(m^3)	
LH-μcoil-2	2.5	7.1 x 10^{-9}	0.11 x 10^{-9}	0.8 x 10^{-15}	80
	5.0	10 x 10^{-9}	0.16 x 10^{-9}	1.2 x 10^{-15}	120
	7.5	16 x 10^{-9}	0.26 x 10^{-9}	1.8 x 10^{-15}	180
	10	20 x 10^{-9}	0.31 x 10^{-9}	2.2 x 10^{-15}	220

*1: The deposition efficiencies are comparable to thickness of Cu layer specific to bath load. The ICP-detected Cu volume per one *Spirulina* template was divided by 1.0 x 10^{-8} μm^2 in the typical average surface area.

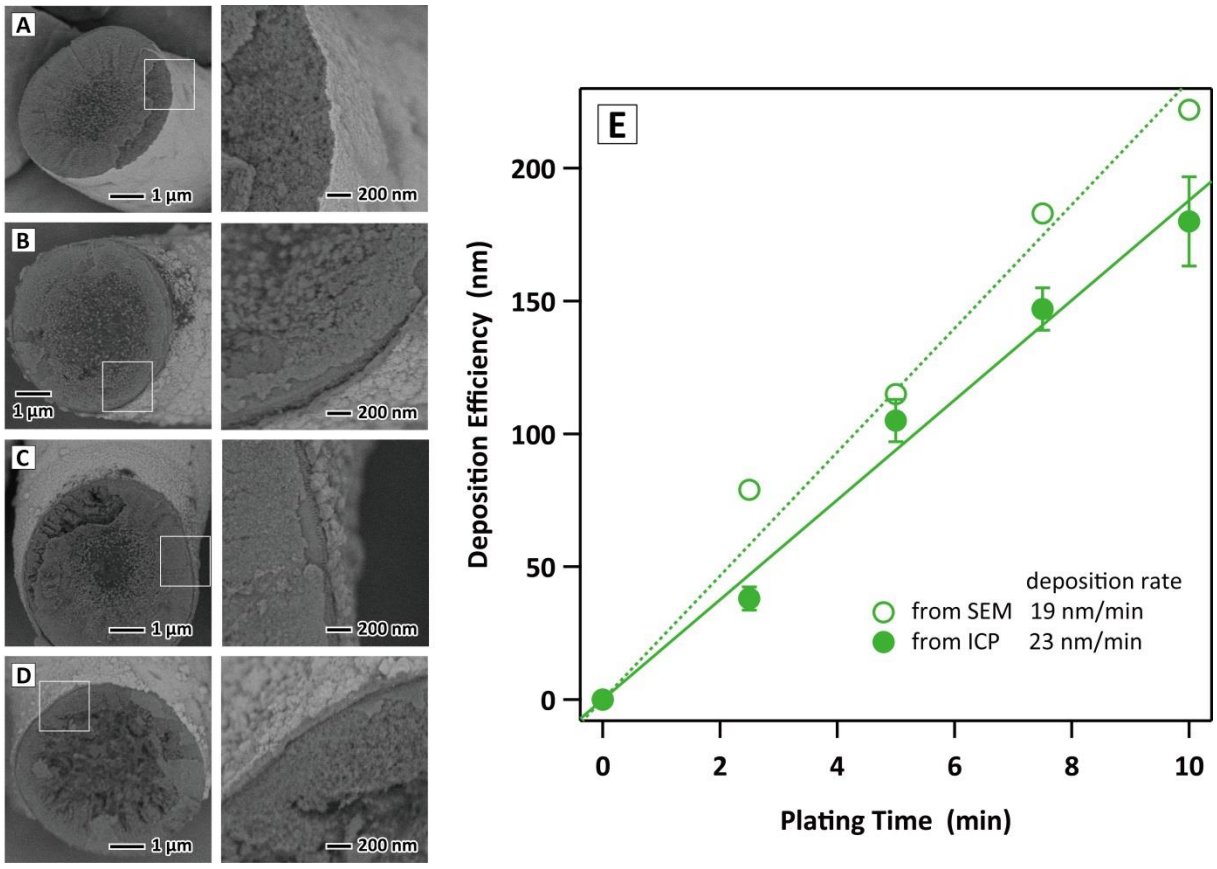

Figure S14 The evaluation of Cu deposition efficiency in the biotemplating process. (A)-(D) SEM images at the cross-sections intentionally produced by collapsing the samples on SEM stages with edge of spatula. The samples were prepared by the plating for (A) 2.5 min, (B) 5.0 min, (C) 7.5 min, and (D) 10 min in the plating time. The right images are magnified at the square areas indicated in the left images. For the detailed measurement of thickness, high-angle back-scattered electron (HA-BSE) mode was used here. (E) The deposition efficiencies are plotted against the plating time in both of the SEM and ICP results.

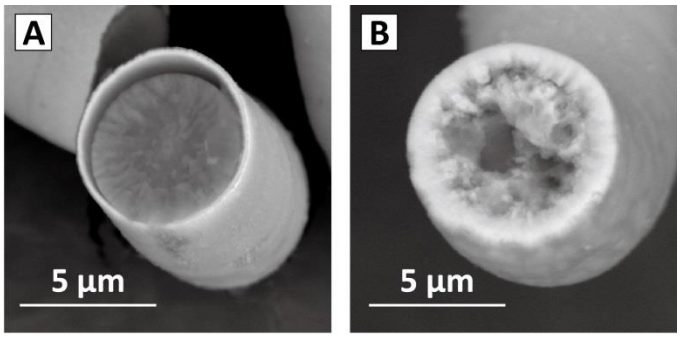

Figure S15 SEM images of Cu µcoils prepared with (A) 400 cm^2/L and (B) 200 cm^2/L in the bath load. The cross-sections were generated by the similar manner to the Fig. S14. The average thickness was changed in the different bath load: (A), 220 nm; (B), 550 nm.

SI-V. Structural parameters of Copper μcoils.

The structural parameters of μcoils were analyzed with the histogram representations (Fig. S16 and S17). The wire diameters (*d*) were reasonably increased because of the Cu layer formation with electroless plating. The *D* and L_{free}/N were sufficiently maintained through the biotemplating process. The L_{free}s became shorter with wide relative standard deviations, which may be attributed to brittle damage of the μcoil happened by stirring for the electroless plating.

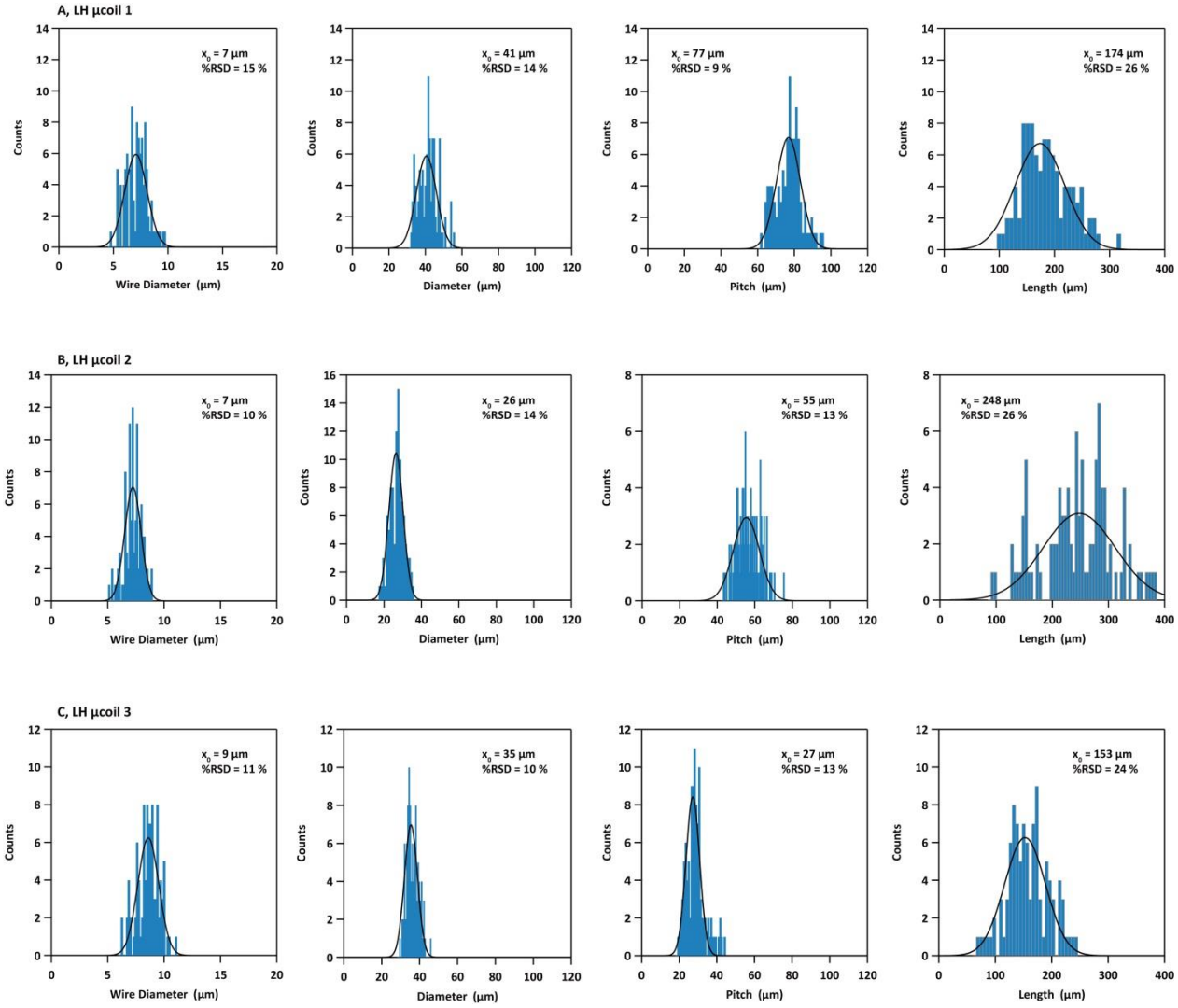

Continued to next page

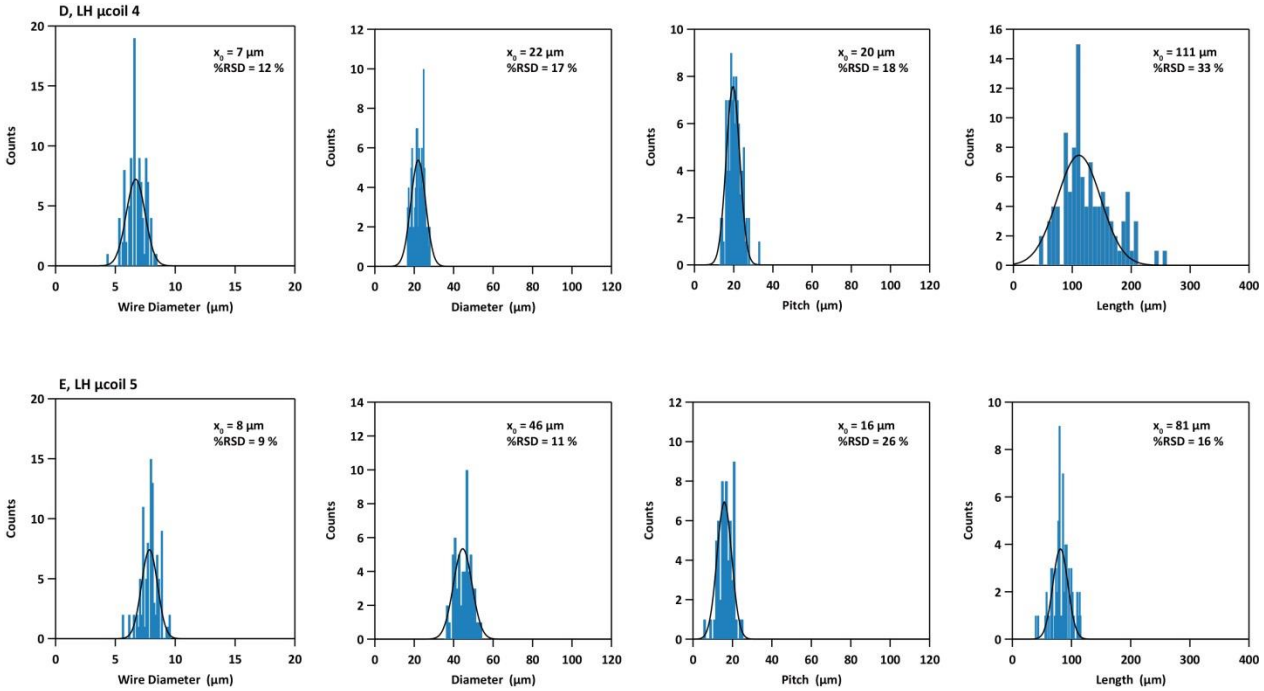

Figure S16 Histograms of structural parameters, wire diameter (*d*), coil diameter (*D*), coil pitch (L_{free}/N), and free length of coil (L_{free}), on helix geometries of LH µcoil-1 to -5. The black lines indicate Gaussian distributions to have averaged values. The average feature size, x_0, and %RSD are indicated in each inset.

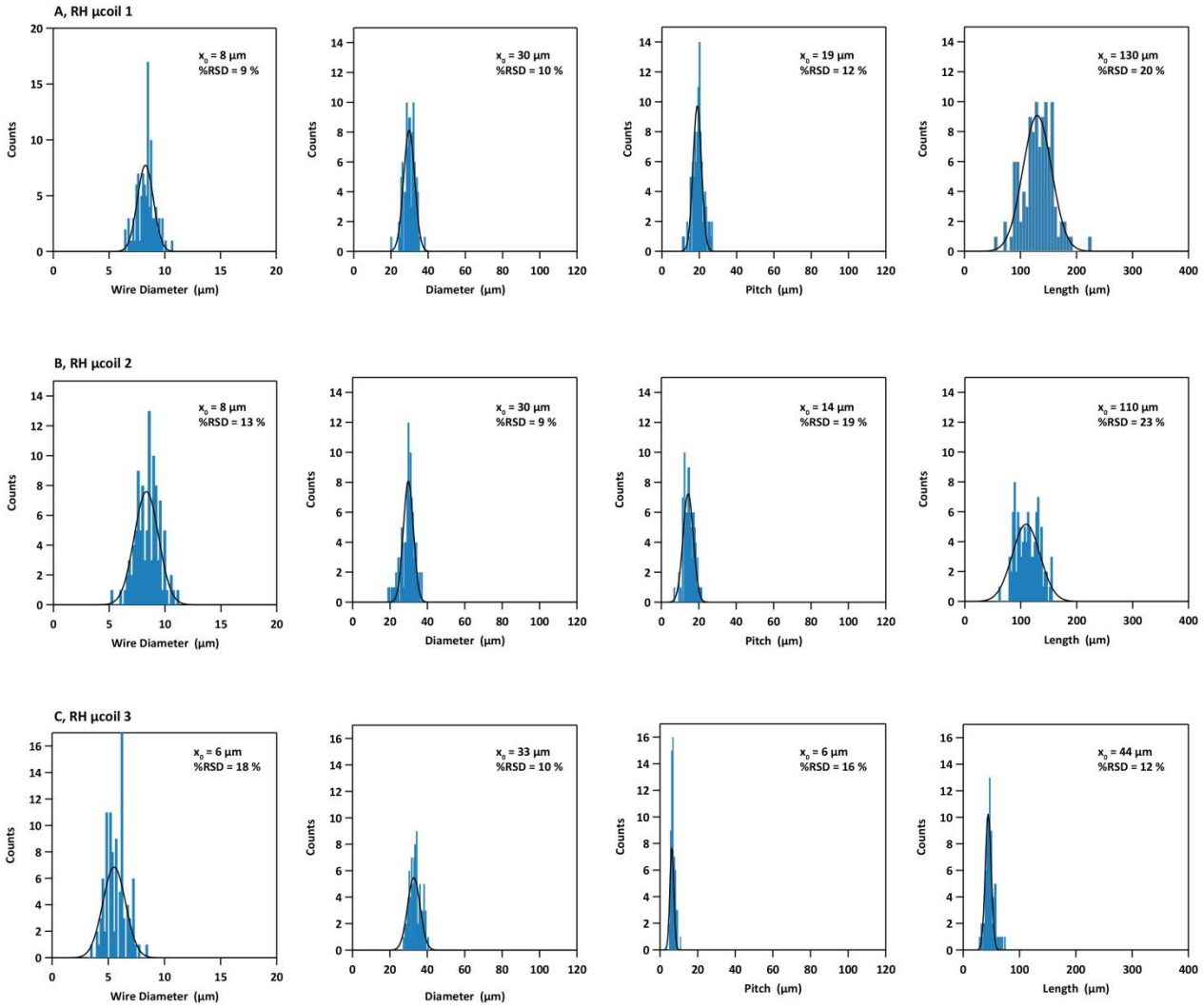

Figure S17 Histograms of structural parameters on helix geometries of RH µcoil-1 to -3.

SI-VI. μcoil-dispersed sheet for evaluation of electromagnetic response

The electromagnetic property within GHz range was analyzed at Japan Fine Ceramics Center. Free space method (S-parameter method) was employed for transmittance and reflectance in the every range of Fig. 4a and 4b; K-band, 18-26.5 GHz; Ka-band, 26.5-40 GHz; V-band, 50-75 GHz; W-band, 75-110 GHz.

We prepared μcoil-dispersed sheets by using paraffin (mp 70-80 °C, Sigma-Aldrich) as a transparent matrix. A prescribed amount of μcoils was dispersed into paraffin melt at 90 °C. The uniformly dispersed paraffin melt was solidified in a mold, affording a μcoil-dispersed paraffin sheet with 4 cm square and 1 mm thickness (Fig. S18). A 1 wt % of the μcoil in the paraffin sheet corresponds to from 10^{11} to 10^{12} coils m^{-3} in number density. The above procedure allowed us to suppress <10 % of entangled μcoils as so-called lump, which causes undesirable contributions in the measurements. The paraffin-based sheets were used for the K- and Ka-bands, and THz wave region. For the V- and W-bands, silicon matrix was used for the fabrication of sheet with 30 cm square and 1 cm thickness.

Figure S18 The photo of μcoil-dispersed paraffin sheets.

The optical densities of μcoil-dispersed paraffin sheets were converted from the transmittances shown in Fig. 4C of the main text (Fig. S19). The intensities at 1.0 THz were plotted against the number densities of μcoils in the paraffin sheets. Since the linear relationship was reproduced with its slope of *ca*. 1.5×10^{-12} with less than 4 % of relative standard deviation, the dispersibility of μcoils into paraffin was guaranteed.

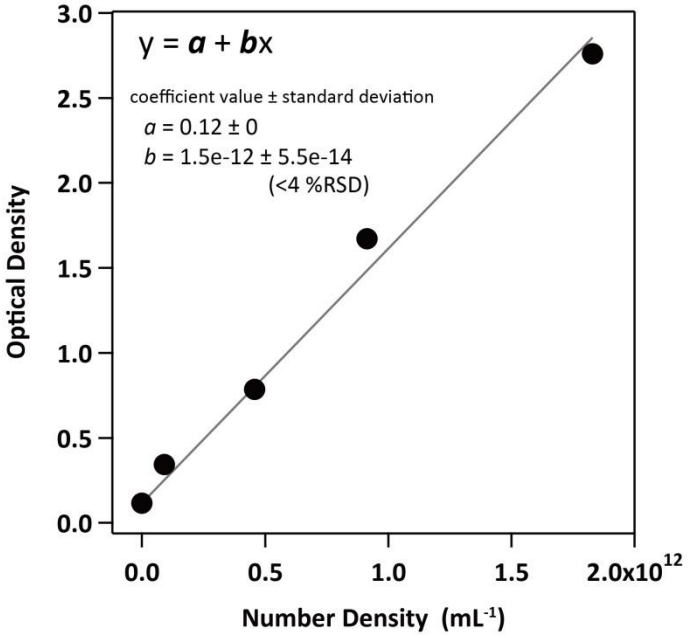

Figure S19 Optical density of LH µcoil-1 at 1 THz as a function of the number density in the paraffin sheet. The optical densities were obtained by conversion from the transmittances shown in Fig. 4C of main text. The solid line indicates line approximation with small error (<4 %RSD).

The normal mode transmission spectra (non-polarization mode) corresponding to Figure 5a were summarized in Figure S20. Every sample shows low transmittance less than 10 %, while the loose LH µcoil-1 is only significant in regard to very low transmittance reaching to 0.01%.

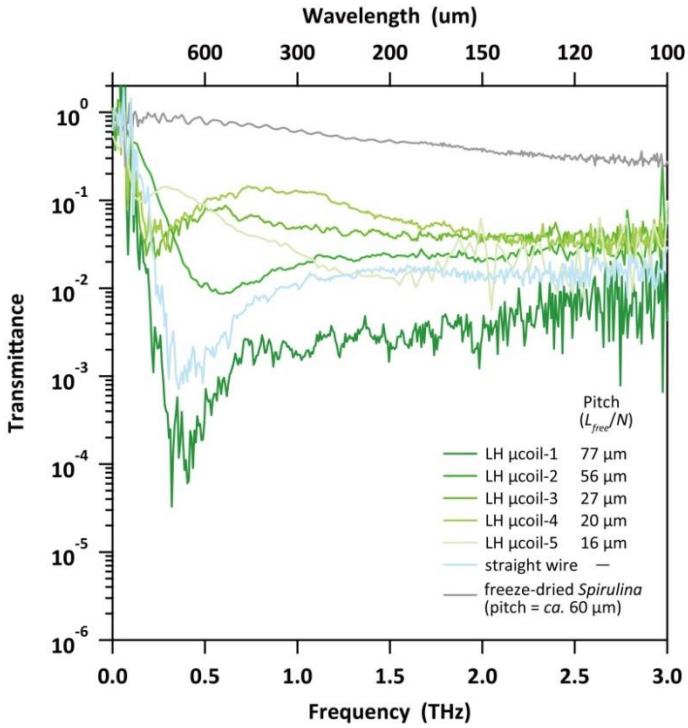

Figure S20 Transmission spectra of series of LH µcoil under non-polarization mode. The sample concentration was 2 wt% in every cases.

SI-VII. THz-TDS-PA setup

A transmission-type THz-TDS system combined with polarimetric analysis was conducted to evaluate the electromagnetic response of Cu μcoils. Femtosecond laser pulses from mode-locked Ti:sapphire laser with pulse width of 100 fs, center wavelength of 800 nm, and time average power of 5.0 mW irradiated gaps of photoconductive dipole antenna fabricated on low-temperature-grown GaAs substrate. The emitter dipole antenna was a.c. biased at 40 V and 3 kHz to generate THz pulses ranging from 0.2 THz to 3.0 THz. The emitted THz wave was collimated by an off-axis paraboloidal reflector to propagate through the sample toward a second paraboloidal reflector. The focused THz wave reached to the detector dipole antenna, which was triggered by gate pulse separated from the laser pulse through optical time delay stage. For the polarization analysis, three wire grid polarizers (WG1 to WG3) were inserted: WG1, between the emitter and the sample to linearly polarize the THz wave; WG2, between the sample and WG3 with +45 ° or -45 ° against the horizontal direction to analyze the polarization of THz wave transmitted through the sample; WG3, between WG2 and the detector to extract the polarization component parallel to the most sensitive direction for the detector. By scanning the time delay stage, the time evolution of the polarization state of THz wave transmitted from the samples were obtained. Transmission intensities of left- and right- handed circular polarizations (LCP, RCP) with their phase shifts are obtained from the x- and y-axis components (E_x and E_y) of the transmitted THz waveforms in the time domain. The Fourier transformation applied to the transmitted THz wave derived the transmission spectra, ellipticity, γ, and rotation angle, η, in the frequency domain.

In order to define the sense of rotation of emitted elliptical polarization, it should be noted that the transmitted wave was observed *against* the direction of propagation from the detector, *i.e*., the complex amplitude of the RCP and LCP of the THz waves, E_R and E_L are obtained as $E_R = \frac{1}{\sqrt{2}}(E_x - iE_y)$ and $E_L = \frac{1}{\sqrt{2}}(E_x + iE_y)$, respectively. Here, the phase of the THz wave is defined by $\theta = \omega t - kz + \phi$, where ω is angular frequency, k is wave vector, and ϕ is phase. The polarization state is described with $\tan\gamma = \frac{|E_R| - |E_L|}{|E_L| + |E_R|}$ and $\eta = \frac{1}{2}\arg\frac{E_L}{E_R}$.

As became clear above, the spectrum obtained from THz-TDS under non-polarization mode should trace an average of those against LCP and RCP in polarization mode, THz-TDS-PA.

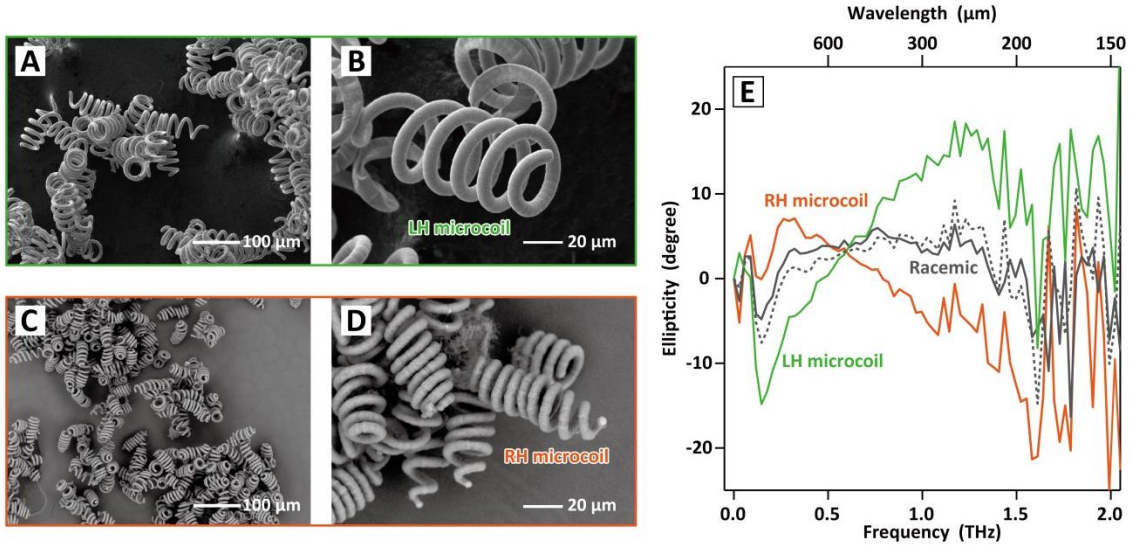

Figure S21 Dependence of µcoil handedness on ellipticity spectra. SEM images of (**A**), (**B**) LH µcoil-5 and (**C**), (**D**) RH µcoil-2. (**E**) Ellipticity spectra of LH (green line), RH (orange line) µcoils, and racemic mixture (gray solid line) with 2 wt% of concentration for all the samples. The average spectrum of ellipticities of LH and RH µcoils is also added in dotted gray line. The LH and RH µcoils afforded nearly mirror-image ellipticity spectra over the full spectral range, while the racemic mixture showed almost flat spectral feature.

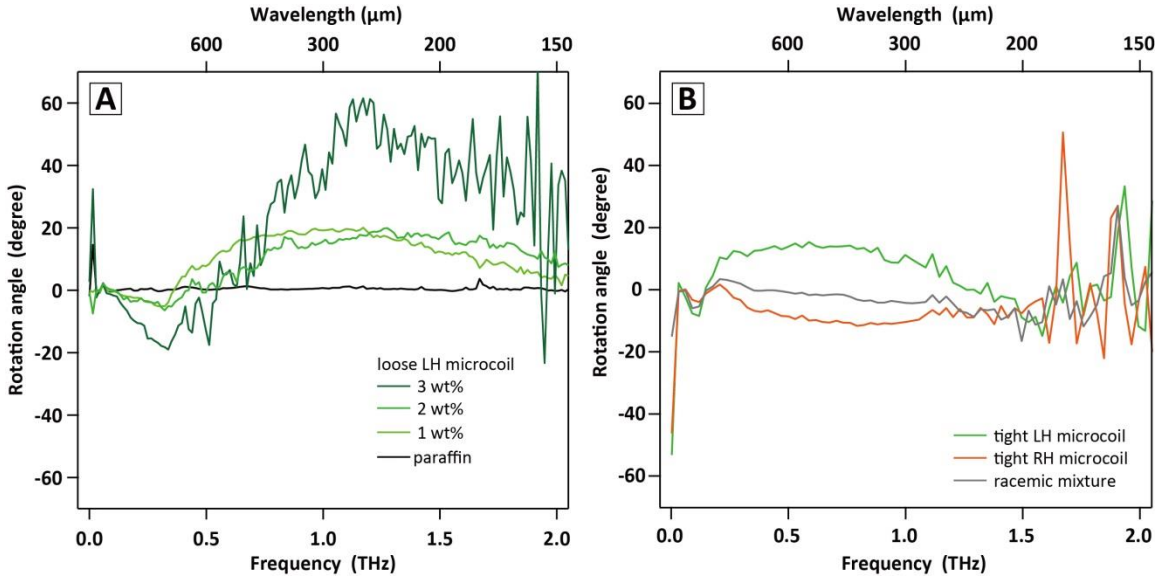

Figure S22 Rotation angle spectra of µcoil sheets including (A) loose LH µcoil-2 with different weight concentrations and (B) the enantiomeric pair of LH µcoil-5 and RH µcoil-2 (2 wt%).

The handedness of μcoil was firmly identified by SEM observation (Fig. S21A to S21D). Correspondent pair of LH and RH μcoils in respect to L_{free}/N and D was selected to examine the optical chirality, *i.e.*, LH μcoil-5 and RH μcoil-2. This enantiomeric pair exhibited ellipticity spectra with opposite sign, while the observable ellipticity disappeared for racemic form intentionally mixed with two of them (Fig. S21E). The racemic mixture resulted in being offset the ellipticity expressed by the handedness of μcoil.

The rotation angle spectra were also obtained for the same series as the above experiment (Fig. S22). It can be confirmed that the LH and RH μcoils showed dextrorotation and laevorotation, respectively. Since the μcoil effectively absorbs circularly-polarized wave rotating to the same direction as the handedness of μcoil, the oppositely-rotating circular polarization only can transmit through the μcoil-dispersed sheet.

SI-VIII. Geometric parameters of samples

Table S3 The geometric parameters of LH μcoils and predictable operation frequencies

Parameters	symbol	Units	LH μcoil-1	LH μcoil-2	LH μcoil-3	LH μcoil-4	LH μcoil-5
wire diameter	d	μm	7	7	9	7	8
coil diameter	D	μm	41	26	35	22	46
free length of pitch	L_{free}/N	μm	77	56	27	20	16
number of turn	N	-	2.3	4.5	5.7	5.6	5.1
free length of coil	L_{free}	μm	174	248	153	111	81
length of wire for one pitch	L_{wire}/N	μm	150	99	113	72	145
length of wire for one coil	L_{wire}	μm	339	441	642	399	736
cross-sectional area of Cu layer[1]		m^2	13 x 10^{-12}	13x 10^{-12}	16 x 10^{-12}	13 x 10^{-12}	15 x 10^{-12}
volume of one coil[2]	V_{coil}	m^3	4.4 x 10^{-15}	5.8 x 10^{-15}	11 x 10^{-15}	5.2 x 10^{-15}	11 x 10^{-15}
mass of one coil[3]	M	g/(one coil)	40 x 10^{-9}	52 x 10^{-9}	95 x 10^{-9}	47 x 10^{-9}	97 x 10^{-9}
pitch angle[4]	α	degree	30.9	34.0	13.8	16.1	6.3
theoretical operation frequency (pitch)[5]	F_d	THz	0.67-1.33	1.02-2.03	0.88-1.77	1.39-2.78	0.69-1.38
(total length)		THz	0.29-0.59	0.23-0.45	0.16-0.31	0.25-0.50	0.14-0.27
experimental frequency range[6]		THz	0.5-1.5	0.5-1.6	0.5-1.9	0.5-2.1	0.4-1.2

[1]The cross-section is ring-shape consisting of Cu layer with 550 nm thickness. [2]The V_{coil} only includes volume of Cu shaping one coil. [3]The M is obtained by multiplying V_{coil} by theoretical density of Cu metal, 8.94 x 10^6 g/m^3. [4]The pitch angle equals to $\tan^{-1}(L_{free}/N) / (\pi D)$. [5]The region of frequency means that the μcoil emits elliptical polarization with the opposite handedness within the range and can be predicted with $L_{wire}/N < \lambda_0 < 2L_{wire}/N$, as defined in helical antenna array. The wave propagates in paraffin matrix (n = 1.5), so that the operation frequency is given by $F_d = \frac{300 \times n}{\lambda_0}$. [6]The frequency region was defined as the difference between two peaks of ellipticity angles.

Table S4 The geometric parameters of RH μcoils and predictable operation frequencies

Parameters	**symbol**	**Units**	**RH μcoil-1**	**RH μcoil-2**	**RH μcoil-3**	**Straight wire**[1]	**Freeze-dried *Spirulina***[2]
wire diameter	d	μm	8	8	6	6	5
coil diameter	D	μm	30	30	33	*n/a*	20
free length of pitch	L_{free}/N	μm	19	14	6	*n/a*	44
number of turn	N	—	6.8	7.9	7.0	*n/a*	4.3
free length of coil	L_{free}	μm	130	110	44	320	188
length of wire for one pitch	L_{wire}/N	μm	96	95	104	*n/a*	77
length of wire for one coil	L_{wire}	μm	658	749	725	320	328
cross-sectional area of Cu layer		m^2	15×10^{-12}	15×10^{-12}	11×10^{-12}	11×10^{-12}	*n/a*
volume of one coil	V_{coil}	m^3	9.7×10^{-15}	11×10^{-15}	8.2×10^{-15}	3.6×10^{-15}	*n/a*
mass of one coil	M	g/(one coil)	87×10^{-9}	99×10^{-9}	73×10^{-9}	32×10^{-9}	*n/a*
pitch angle	α	degree	11.4	8.5	3.5	90	35
operation frequency in paraffin (pitch)	F_d	THz	1.04-2.08	1.05-2.10	0.96-1.93	*n/a*	1.30-2.61
(total length)		THz	0.15-0.30	0.13-0.27	0.14-0.28	0.31-0.63	0.31-0.61
experimental frequency range		THz	0.4-1.6	0.3-2.0	*n/a*	*n/a*	*n/a*

[1]The sample formed straight shape, so that V_{coil} and M were described as the volume and mass of Cu wire, respectively. [2]The F_d values were simply obtained from the sample shape regardless of the presence or absence of Cu metal coating (electroconductivity). The *n/a* indicates the parameter inapplicable to the sample.

1 Fiermans, L., Gryse, R. D., Doncker, G. D., Jacobs, P. A. & Martens, J. A. Pd Segregation to the Surface of Bimetallic Pt-Pd Particles Supported on H-β Zeolite Evidenced with X-Ray Photoelectron Spectroscopy and Argon Cation Bombardment. *J. Cat.* **193**, 108-114 (2000).

2 Ghijesen, J. et al. Electronic structrue of Cu_2O and CuO. *Phys. Rev. B* **38**, 11322-11330 (1988).